**Aluminium distribution in an Earth's non–primitive lower mantle**

Dear author,

Please note that changes made in the online proofing system will be added to the article before publication but are not reflected in this PDF.

We also ask that this file not be used for submitting corrections.

Available online at www.sciencedirect.com
ScienceDirect
Geochimica et Cosmochimica Acta xxx (2020) xxx–xxx
Geochimica et Cosmochimica Acta
www.elsevier.com/locate/gca

# Aluminium distribution in an Earth's *non–primitive* lower mantle

Marcello Merli [a], Costanza Bonadiman [b,*], Alessandro Pavese [c]

[a] *Department of Earth and Marine Sciences, University of Palermo, Via Archirafi 36, 90123 Palermo, Italy*
[b] *Department of Physics and Earth Sciences, University of Ferrara, Via Saragat 1, 44122 Ferrara, Italy*
[c] *Department of Earth Sciences, University of Turin, Via Valperga Caluso 32, 10100 Turin, Italy*

Received 26 September 2019; accepted in revised form 20 February 2020; available online xxxx

**Abstract**

The aluminium incorporation mechanism of perovskite was explored by means of quantum mechanics in combination with equilibrium/off-equilibrium thermodynamics under the pressure-temperature conditions of the Earth's lower mantle (from 24 to 80 GPa). Earth's lower mantle was modelled as a geochemically *non-primitive* object because of an enrichment by 3 wt% of recycled crustal material (MORB component). The compositional modelling takes into account both chondrite and pyrolite reference models.

The capacity of perovskite to host Al was modelled through an $Al_2O_3$ exchange process in an unconstrained Mg-perovskite + Mg-Al-perovskite + free-$Al_2O_3$(corundum) system. Aluminium is *globally* incorporated principally *via* an increase in the amount of Al bearing perovskite [*Mg-Al-pv*(80 GPa)/*Mg-Al-pv*(24 GPa) ≈ 1.17], rather than by an increase in the $Al_2O_3$ content of the average chemical composition which changes little (0.11–0.13, mole fraction of $Al_2O_3$) and tends to decrease in Al. The $Al_2O_3$ distribution in the lower mantle was described through the probability of the occurrence of given compositions of Al bearing perovskite. The probability of finding Mg-Al-perovskite is comparable to Mg-perovskites. Perovskite with $Al_2O_3$ mole fraction up to 0.15 has an occurrence probability of ~28% at 24 GPa, increasing up to ~43% at 80 GPa; on the contrary, perovskite compositions in the range 0.19–0.30 $Al_2O_3$ mole fraction drop their occurrence probability from 9.8 to 2.0%, over the same *P*-range. In light of this, the distribution of Al in the lower mantle shows that, among the possible Al bearing perovskite phases, the $(Mg_{0.89}Al_{0.11})(Si_{0.89}Al_{0.11})O_3$ composition is the likeliest, providing from 5 to 8% of the bulk perovskite in the pressure range from 24 to 80 GPa. The occurrence of the most Al rich composition, *i.e.* $(Mg_{0.71}Al_{0.29})(Si_{0.71}Al_{0.29})O_3$, is a rare event (probability of occurrence < 1.7%). This study predicts that perovskite may *globally* host $Al_2O_3$ in terms of 4.3 and 4.8 wt% (with respect to the *non-primitive* lower mantle mass), thus accounting for ~90% and 100% of the bulk $Al_2O_3$ estimated in the framework of pyrolite and chondrite reference models, respectively. A calcium-ferrite type phase (on the $MgAl_2O_4$-$NaAlSiO_4$ join) seems to be the only candidate that can compensate for the 10% gap of the perovskite Al incorporation capacity, in the case of a pyrolite *non-primitive* lower mantle model.


*Keywords:* Aluminium distribution; Earth's lower mantle; Aluminium bearing perovskite; Pyrolite; Chondrite reference model; MORB component; Enriched lower mantle composition; Open system

## 1. INTRODUCTION

The mantle is the Earth's largest division by volume, originally marked by a planetary Siderophile/Lithophile element fractionation. Refractory Lithophile Elements (RLE) condensed from a gas of solar nebula composition at the highest temperature (>1400 K at $10^{-4}$ atm) compatible with

* Corresponding author.
*E-mail address:* costanza.bonadiman@unife.it (C. Bonadiman).

https://doi.org/10.1016/j.gca.2020.02.023
0016-7037/

the nebula's physical constraints (Lodders, 2003). RLEs' chemical behaviour prevented metal and sulphide phases from entering both chondrites and metallic cores during the planetary differentiation (Lodders, 2003; Kaminski and Javoy, 2013; Mahan et al., 2018). RLEs include Ca and Al among the major elements, the full group of rare earth elements (REE), U and Th. The chemical characteristics of such elements support the primitive Earth's mantle model that preserves the solar ratios of RLEs (Wasson and Kallemeyn, 1988; Lodders et al., 2009; Wang and Jacobsen, 2016).

Aluminium is the sixth most abundant element on Earth: it is a purely refractory lithophile element and its natural abundance is provided by the stable isotope $^{27}$Al. The radioactive isotope $^{26}$Al quickly decayed to $^{26}$Mg ($^{26}$Al half-life $= 7.17 \pm 0.24 \times 10^5$ yr; Norris et al., 1983, Wu and Browne, 1997) during the early stage of the solar system's evolution (Lee et al., 1977; Lodders, 2003; Baker et al., 2012). The $^{26}$Al decay provided substantial heating to the proto planetary bodies, and its isotopic daughter is one of the most widely used extinct radioactivity chronometers (Bizzarro, et al., 2005; Spivak-Birndorf et al. 2009; Wimpenny et al., 2019).

Considering the geochemical behaviour of aluminium, it is unlikely that a large amount of such element may enter the Earth's core, though it provides a major constituent of many minerals at any depth of the Earth's mantle and crust. Aluminium is also one of the main components of any melt generated from the upper mantle, in terms of 9–21 wt% $Al_2O_3$ on average (source: PetDB Petrological Database). Melt crystallization, segregation, rise and cooling, led to the formation of the crust over the Earth's history. An intriguing aspect is that Al, as a crustal component, partially, or entirely, was transported into the mantle, through subduction. Such a process could involve mantle portions well below the magma source regions (Young et al., 2005; Tsuchiya and Tsuchiya, 2008; Wang and Jacobsen, 2016).

Seismic tomography reveals that near the Earth's mantle transition zone, which marks the boundary between upper and lower mantle, repositories of crustal material occur (Christensen and Yuen, 1984; Billen, 2010, King et al., 2015). They exhibit different dynamic behaviours: (i) stagnation in the mantle transition zone (Japan trench; Honda, 2017 and references therein); (ii) stagnation in the uppermost lower mantle (Peruvian Andes; Fukao and Obayashi 2013); (iii) continuous descent, seemingly unhindered, into the lower mantle (Farallon plate, North America; Sigloch et al., 2008). Such tomographic observations suggest a mechanism of global mantle convection with an abundant mass exchange between distinct geochemical reservoirs lying in both the upper and lower mantle (van der Hilst et al., 1997; Nolet et al., 2007).

More recently, geochemical models, aimed at explaining the isotopic evolution of the silicate Earth (Kumari et al., 2016; Jones et al., 2019) or at tracing the distribution of key components ($H_2O$ and Fe-Mg) in the lower mantle (Walter et al., 2015; Merli et al., 2016, 2017), have depicted the Earth's mantle as a chemical reservoir (pyrolite) involving uninterrupted geochemical reactions and energy/matter flows.

In particular, Kumari et al. (2016) estimated that about 60% of the entire mantle is as depleted in fusible elements (*i.e.* Al and Ca) as its upper portion, whereas the remaining mantle is *non-primitive*, containing a small fraction of transient and isolated recycled crustal materials.

Jones et al. (2019), combining the geodynamic model of mantle convection with isotope and trace element geochemistry, suggest that the subduction and accumulation of dense oceanic crust produce in the deep mantle a large mass of material enriched in incompatible trace elements. The quoted authors also state that an equivalent of 50–70% of the current continental crust mass was accumulated earlier than 3 Ga ago, and that the crustal recycling and reworking dominated over juvenile additions to the continental crust, since the end of the Archean (2.5 Ga). This suggests that since the end of the Hadean age (~4.6–3.8 Ga) the Earth's lower mantle has been enriched with crustal components.

Understanding the structure and chemical-physical behavior of the slabs subducted into the mantle is out of the scope of the present work. Conversely, we focus on the chemical rearrangement of the main lower mantle mineral phases in the case of a full mixing between crustal slabs and primordial lower mantle. In such a view, aluminum may be an effective "*probe*" among the major elements.

The present work deals with the modelling of Al incorporation in perovskite, the major phase in the lower mantle, and the resulting Al distribution, by means of quantum mechanics calculations in combination with equilibrium/off-equilibrium thermodynamics and cluster expansion technique. The cluster expansion approach allows the investigation of large atom clusters, thus providing an effective tool to model solid mixing in a statistical framework (see Merli et al., 2015, and references therein). Because of the complexity of the natural processes, it is convenient to start from a "reference" mineral phase, *i.e.* $MgSiO_3$-perovskite, whose Al enrichment is investigated. We explore the *P*-range from 24 to 80 GPa, to unquestionably leave the perovskite to post perovskite transition aside (Murakami et al., 2004; Tsuchiya and Tsuchiya, 2008; Shim et al., 2008).

Our main goal is to estimate the maximum intrinsic capacity of perovskite to incorporate aluminium and its phase proportion with respect to the Al free perovskite fraction, as a function of *P-T*. Subsequently, the resulting Al partitioning will be used to discuss the global mechanism of storage of aluminium in the lower mantle.

## 2. GEOCHEMISTRY

### 2.1. Lower mantle geochemical model

Cosmochemical arguments supporting a chondritic bulk Earth composition (chondrite reference model) imply that the lower mantle must be enriched in Si with respect to a primitive upper mantle (PUM; Javoy et al., 2010; Murakami et al., 2012; Kaminski and Javoy 2013), except that the Earth's core should be able to host ~4–6 wt% Si (McDonough, 2014; Badro et al., 2014) to balance the Earth's Si budget against



Please cite this article in press as: Merli M., et al. Aluminium distribution in an Earth's *non–primitive* lower mantle. *Geochim. Cosmochim. Acta* (2020), https://doi.org/10.1016/j.gca.2020.02.023

that of the Sun and chondrite [$Mg/Si_{(PUM)} \sim 1.21–1.31$ *versus* $Mg/Si_{(lower\ mantle)} \sim 1.01$]. Conversely, according to petrological data and chondritic constraints, the lower mantle is chemically equivalent to the primitive upper mantle (pyrolite reference model; McDonough and Sun, 1995; Lyubetskaya and Korenaga, 2007).

Tomographic images of subducted slabs plunging into the deep mantle have been interpreted in terms of an efficient mass transfer between upper and lower mantle domains. This supports large scale mixing and therefore a homogenous Mg/Si distribution (*i.e.* pyrolite) throughout the mantle (Sigloch et al., 2008; van der Hilst et al., 1997). However, only a limited number of slabs sink into the lower mantle, given that most of the subducted slabs flatten and seem to stagnate at either ~660 km or ~1000 km depth (Fukao and Obayashi, 2013). This points towards a comparatively ineffective mixing process and contrasts with the notion of a vigorous global mantle convection. Recently, Ballmer et al. (2017) have hypothesised the presence of stable, large-scale, high-viscosity, bridgmanite-enriched ancient mantle structures (BEAMS) that have been residing in the Earth's lower mantle since the early stage of our planet's formation. Their numerical model also predicts the incorporation of limited amounts of crustal material from shallow to deep mantle, particularly during the early stages. Such crustal portions provide stretched and stirred long-lived "fossil" fragments, in keeping with tomographic observations. Therefore, large-scale heterogeneities may account for the Earth's bulk composition, bringing the lower mantle's Mg/Si ratio closer to the solar-chondritic ratio than that of the upper mantle.

Hereafter, we shall refer to either the "pyrolite model" (based on the pyrolite composition throughout the mantle) or the "chondrite model" (relying on different compositions between upper and lower mantle) to describe the lower mantle.

Whatever bulk composition model is used to interpret the mantle's dynamics, the crustal components plunging into the lower mantle cause large/small-scale changes of its phase composition (Irifune et al., 1996; McDonough, 2016; Nestola et al., 2018).

### 2.2. Enriched (*non-primitive*) lower mantle bulk composition

Both chondrite and pyrolite lower mantle models are used here to estimate the *non-primitive* lower mantle compositions. The bulk chemical composition of the lower mantle is generally described in terms of its five major oxides (MgO, FeO, CaO, $Al_2O_3$ and $SiO_2$), which account for ~98.5 wt% of the Earth's mantle mass (Mc Donough, 2016; Palme and O'Neill, 2014). Although the $Na_2O$ occurrence has a modest impact on the large-scale geophysical and geochemical modelling (Bina and Helffrich, 2014; Palme and O'Neill, 2014; Chust et al., 2017), it is still important in terms of the resulting minor mineral phases that affect the Al distribution in the lower mantle. Experiments and observations on natural samples reveal that potential Al bearing lower mantle phases may also include K, $Fe^{3+}$ and OH as major elements (*i.e.*: Kato et al., 2013; Wang et al., 2015; Pamato et al., 2015; Harte and Richardson, 2012). In particular, Al bearing phases are able to host potassium if they form in a system containing at least ~0.09 wt% $K_2O$ (Kato et al., 2013). Note that the average composition of mid ocean ridge basalt (MORB) has 0.08–0.12 wt% $K_2O$ (Gale et al., 2013), whereas pyrolite and chondrite lower mantle models are estimated to bear ~0.03 and <0.01 wt% $K_2O$, respectively (McDonough and Sun, 1995; Javoy et al., 2010). Therefore, K bearing phases are not expected to play a relevant role as potential aluminum hosts among the lower mantle phases. Although ferric iron is able to affect $Al^{3+}$ storage in perovskite-like structures *via* $Fe^{3+} \leftrightarrow Al^{3+}$ replacement (Kurnosov et al., 2017), the $Fe^{3+}/\sum Fe_{tot}$ ratio in the primitive Earth's mantle is supposed to be very small, *i.e.* ~0.03, according to mass balance calculations (Palme and O'Neill, 2014). Bulk $H_2O$ (hosted as OH-group) in the lower mantle influences the aluminium content incorporated by perovskite through the formation of Al bearing hydrous phases. However, the bulk $H_2O$ content is comparatively modest and estimated ~1500 ppm, in both pyrolite and chondrite lower mantle models (Merli et al., 2016; Muir and Brodholt, 2018).

Let us consider the lower mantle as a geochemically *non-primitive* object because it is mixed with a fraction of recycled crustal material (*i.e.* MORB component). In this view, $Al_2O_3$ and CaO, hosted in lower mantle minerals, are potential "*probes*" which mark the occurrence of such a geodynamic process (Guignot and Andrault, 2004, Hirose et al., 2005; Korenaga, 2009; Irifune et al., 2010; Ricolleau et al., 2010).

The MORB chemical composition is enriched in incompatible major elements (aluminium, calcium and, to a lesser extent, iron) and depleted of compatible elements (magnesium) with respect to the mantle (Table 1). Therefore, a MORB-like composition at lower mantle *P-T* conditions cannot give Fe-periclase, whereas high-pressure $SiO_2$-rich phases (*e.g.* Ca-perovskite and bridgmanite) and additional aluminium rich phases are expected to occur. Following experimental results about MORB bulk compositions (14–16 wt% $Al_2O_3$) under lower mantle conditions (30–90 GPa), the newly formed $Al_2O_3$ rich phases (NAL type phase and $CaFe_2O_4$ type phase, *i.e.* NAL/CF-phase, on the join $MgAl_2O_4$-$NaAlSiO_4$) may account for about 10–12 mol% by phase composition (Guignot and Andrault, 2004, Ricolleau et al., 2010).

Assuming that subducted crustal fragments have been sliding down into the mantle over the past 4 billion years (the most generous estimate is about 11 wt% of the whole mantle; Li and McNamara, 2013), aluminium rich domains should have developed, in contrast to expectations from a primitive lower mantles composition (Stixrude and Lithgow-Bertelloni, 2012).

We model such an enrichment using the simple binary mixing equation of Faure (1986) to combine primitive lower mantle compositions (pyrolite and chondrite, corresponding to the end-members "A" and "A1", respectively; see Table 1) with a crustal type composition



Please cite this article in press as: Merli M., et al. Aluminium distribution in an Earth's *non–primitive* lower mantle. *Geochim. Cosmochim. Acta* (2020), https://doi.org/10.1016/j.gca.2020.02.023

Table 1
Lower mantle (pyrolite, end-member A, and chondrite, end-member A1) and MORB-like silicate glass (end-member B) major oxides compositions. Enriched LM models according to Faure (1986) mixing equation.

| Pyrolitic lower mantle model | A | | B |
|---|---|---|---|
| | | A + 3% B | |
| wt% | | | |
| $SiO_2$ | 45.00 | 45.14 | 49.64 |
| $Al_2O_3$ | 4.45 | 4.76 | 14.88 |
| $FeO_t$ | 8.05 | 8.15 | 11.43 |
| MgO | 37.80 | 36.92 | 8.51 |
| CaO | 3.55 | 3.76 | 10.52 |
| Na2O | 0.36 | 0.44 | 2.90 |
| $H_2O$ | *0.15 | 0.149 | **0.10 |
| *(Mg-pv + Mg-Fe-pv + Mg-Al-pv)*$^+$ | 76.00 | 75.56 | 31.30 |
| Chondritic lower mantle model | A1 | | B |
| | | A1 + 3% B | |
| wt% | | | |
| $SiO_2$ | 47.30 | 47.37 | 49.64 |
| $Al_2O_3$ | 3.99 | 4.31 | 14.88 |
| $FeO_t$ | 8.12 | 8.22 | 11.43 |
| MgO | 37.36 | 36.50 | 8.51 |
| CaO | 2.29 | 2.54 | 10.52 |
| $Na_2O$ | 0.34 | 0.42 | 2.90 |
| $H_2O$ | *0.15 | 0.149 | **0.10 |
| *(Mg-pv + Mg-Fe-pv + Mg-Al-pv)*$^+$ | 85.00 | 84.89 | 31.30 |

End member A from McDonough and Sun (1995).
End member A1 from Merli et al. (2016), modified.
End member B = MORB-like silicate glass of Hirose et al. (1999).
$^+$ = global estimates (wt%) of pure perovskite (*Mg-pv*), bridgmanite (*Mg-Fe-pv*) and Al beraring perovskite (*Mg-Al-pv*).
$^*$ = lower mantle water estimates from Merli et al. (2016) andMuir and Brodholt (2018).
$^{**}$ = MORB water estimates from Ghosh et al. (2014) and Marty (2012).

(end-member "B"; MORB-like silicate glass; see Table 1). End-member B is close to the N-MORB average of Gale et al. (2013) and has been largely used in H*P* experiments (*i.e.* Hirose et al., 1999, 2005; Funamori et al., 2000; Guignot and Andrault, 2004; Ricolleau et al., 2010). According to the extensive compilation provided by the PetDB-database of chemical data from mid-ocean ridge basalts, the water concentrations lie in the range 0.05–1.0 wt%. The amount of $H_2O$ stored in the deep mantle, computed by experiments and mass balance models (Ghosh et al., 2014; Marty, 2012), is in the range 800–2700 ppm (*i.e.* 0.08–0.27 wt%). Taking into account such figures and the tomographic observations that suggest that only small fractions of descending slabs reach the lower mantle (Ballmer et al., 2017), we model a *non-primitive* lower mantle composition by a chemical mixing of primitive pyrolite/chondrite compositions with a 3 wt% end-member B's contribution (0.1 wt% of $H_2O$). The resulting compositions are reported in Table 1. Such chemical mixing ideally reproduces a *non-primitive* lower mantle as predicted by modelling the isotopic evolution of the silicate Earth: ~3 wt% of the total mantle mass is expected to be stored and ultimately mixed within ~1 Ga in the lower mantle (Christensen and Hofmann, 1994; Kumari et al., 2016; White, 2015).

## 3. METHODS

### 3.1. Chemical probability of formation: aluminium bearing phases in the lower mantle

The probability that a phase "J" forms at *P-T*, *i.e.* $p(J|P,T)$, can be roughly estimated in terms of $p(J|P,T) \propto p(J,\text{chem}) \times \exp(-\Delta G(P,T)_{\text{formation}}/RT)$, where $p(J,\text{chem})$ is the probability of having the required chemical species for J under the constraint of a given available elemental budget and $\Delta G(P,T)_{\text{formation}}$ is the formation Gibbs energy. $p(J,\text{chem})$ is termed "*chemical probability of formation*", to underline that it reflects the likelihood of having the required elements to form the J-phase, and it is calculated as follows.

Let us assume $X_k$ to represent the fractional abundance value of the $k^{\text{th}}$ oxide, in a generic system. Given that

$$\sum_{k=1,M} X_k = 1 \quad (1)$$

then $X_k$ can also be associated with the *probability* of having the $k^{\text{th}}$ oxide, if the oxides are supposed to be uniformly distributed as a function of space. The chemical composition of the J-phase is then expressed formally as

$$J = \sum_k n_k X_k \quad (2)$$

Therefore, the probability of finding one mole of the J-phase as a function of its pure chemical composition, $p$(J, chem), is provided by the joint events of (i) having ($n_1$ moles of $X_1$)($n_2$ moles of $X_2$)…. and (ii) not having any species with stoichiometric coefficient equal to 0. This corresponds to the following joint probability:

$$p(\mathrm{J},\mathrm{chem}) \propto \prod_k p(k)^{n_k} \times \left(1 - \sum_m p(m)\right) \propto \prod_j X_j^{n_j} \times \left(1 - \sum_m X_m\right) \quad (3)$$

where $p(k)$ and $p(m)$ are the probabilities of finding the $k^{\mathrm{th}}$ and $m^{\mathrm{th}}$ oxide, respectively; the subscript $k$ is associated with the chemical species with stoichiometric coefficients other than zero, whereas $m$ is related to those with stoichiometric coefficients equal to zero. The $p$(J,chem) values calculated in this way are then normalized so that their sum yields unity.

Table 2 reports major phases and potential Al bearing phases that experiments, numerical modelling and exceptional observations on natural findings indicated as possible minerals in a *non-primitive* lower mantle (Table 1).

Preliminary calculations led us to rule out periclase as a host of aluminium, except that the Al incorporation takes place with the contribution of H (Merli et al., 2016). In such a case, the amount of Al involved would be negligible. Panero et al. (2006) estimated regular solution parameters of 12 and 66 kJ/mol for perovskite and akimotoite, respectively. Taking into account (i) the significantly lower energy for Al incorporation in perovskite than in akimotoite and (ii) the restricted range of occurrence of the latter (Panero et al., 2006), we exclude akimotoite as a possible competitor to uptake Al in the *P-T* region under investigation (Stebbins et al., 2001; Li et al., 2008; Tschauner et al., 2018). Majorite garnet, which is the main host of aluminium in the mantle transition region in both pyrolite and basaltic compositions (Irifune and Ringwood, 1993; Litasov and Ohtani, 2007), is transformed into Mg-perovskite + Ca-perovskite at pressures corresponding to the uppermost lower mantle. Experiments show that aluminium is mostly incorporated by Mg-perovskite/bridgmanite in pyrolite or chondrite compositions under lower mantle *P-T* conditions (Irifune et al., 1996; Ricolleau t al., 2008), whereas separate aluminous phases form in basaltic compositions (Hirose et al., 1999; 2005) at the same *P-T* conditions.

In a *non-primitive* lower mantle, aluminium is partitioned between perovskite/bridgmanite and minor Al bearing phases, such as:

i) alkali rich NAL structure phases, like those on the join $NaMg_2Al_{4.8}Si_{1.15}O_{12}$-$KMg_2Al_{4.8}Si_{1.15}O_{12}$ (Gasparik et al., 2000; Kato et al., 2013; Wu et al., 2016). However, as stated above, K bearing phases are unlikely to develop in the lower mantle because of the lack of a sufficient amount of potassium;
ii) CF structure and NAL structure polymorphs, on the join $MgAl_2O_4$-$NaAlSiO_4$ (Imada et al., 2011; 2012; Irifune et al., 1991). Note that the CF structure was observed to stabilize at a higher pressure (∼ >40 GPa) than the NAL-structure (∼24–40 GPa) (Imada et al., 2011; Guignot and Andrault, 2004);
iii) possible hydrous solid solutions involving D-phase, H-phase and δ-AlOOH (Ghosh and Schmidt, 2014; Pamato et al., 2015; Walter et al., 2015; Fukuyama et al., 2017).

In the case of NAL and CF phases, we chose to calculate a *chemical probability of formation* $p$(J,chem) for a reference NAL/CF mineral, that is $Na_{0.265}Fe_{0.245}Mg_{0.375}Ca_{0.035}Al_{1.1}$-

Table 2
Probability, expressed in %, of having the appropriate elemental availability to form a given phase (*chemical probability of formation* = $p$(J, chem); see Section 3.1). Calculations are carried out by pyrolite (A) and chondrite (A1) lower mantle reference models, and by their compositions mixed with 3 wt% of MORB component (A + 3%B; A1 + 3%B).

| | | Pyrolite | | Chondrite | |
|---|---|---|---|---|---|
| Phase name | Composition | A | A + 3%B | A1 | A1 + 3%B |
| Fe-periclase | $(Mg_{0.8}Fe_{0.2})O$ | 33.59 | 33.24 | 32.22 | 31.91 |
| Ca-perovskite | $CaSiO_3$ | 0.674 | 0.745 | 0.452 | 0.523 |
| Mg-perovskite | $MgSiO_3$ | 23.89 | 23.84 | 24.63 | 24.55 |
| Bridgmanite | $(Mg_{0.9}Fe_{0.1})SiO_3$ | 20.76 | 20.83 | 21.44 | 21.49 |
| Mg-Al-perovskite | $(Mg_{0.9}Al_{0.1})(Si_{0.9}Al_{0.1})O_3$ | 20.24 | 20.41 | 20.49 | 20.66 |
| Sum | | **64.90** | **65.08** | **66.56** | **66.70** |
| δ-phase[1] | AlO(OH) | 0.052 | 0.058 | 0.044 | 0.049 |
| H-phase[2] | $(MgSi,Al_2)O_4H_2$ | 0.045 | 0.047 | 0.043 | 0.045 |
| D-phase[3] | $Al_2SiO_4(OH)_2$ | 0.002 | 0.002 | 0.002 | 0.002 |
| NAL/CF[4] | $Na_{0.265}Fe_{0.245}Mg_{0.375}Ca_{0.035}Al_{1.1}Si_{0.715}O_4$ | 0.737 | 0.825 | 0.679 | 0.769 |
| Sum | | 0.836 | 0.932 | 0.768 | 0.865 |

End-member A from McDonough and Sun (1995).
End-member A1 from Merli et al.(2016), modified.
End-member B = MORB-like silicate glass of Hirose et al. (1999).
[1] Ohtani et al. (2001).
[2] Ohtani et al. (2014).
[3] Pamato et al. (2015).
[4] Guignot and Andrault (2004).

$Si_{0.715}O_4$. Such a composition is obtained from Guignot and Andrault (2004), by averaging those that the authors labelled with "$CF^{A}$" and "$CF^{B1}$", neglecting Ti and normalizing to 4 oxygen atoms and 3 cations.

Hereafter we shall use the following acronyms, for the sake of brevity: *Mg-pv*, "Mg-perovskite", for pure perovskite, *i.e.* MgSiO3; *Mg-Al-pv*, "Al-perovskite", for Al bearing Mg-perovskite, *i.e.* $(Mg,Al)(Si,Al)O_3$; *Mg-Fe-pv*, "bridgmanite", for Fe bearing Mg-perovskite, *i.e.* $(Mg,Fe)SiO_3$; *Ca-pv*, "Ca-perovskite", for Ca bearing perovskite, *i.e.* $(Ca,Mg)SiO_3$; "perovskite", for any solid mixing, or end member, occurring in the lower mantle and having perovskite type structure; *Fe-pe*, "Fe-periclase", *i.e.* (Mg,Fe)O; *CF*, "CF-phase", for a phase in the $MgAl_2O_4$-$NaAlSiO_4$ join.

### 3.2. Aluminium incorporation mechanisms of perovskite

To evaluate the aluminium distribution in a *non-primitive* lower mantle, we model the Al uptake capacity of perovskite, which is the lower mantle phase able to host aluminium to such an extent as to provide a relevant storage by volume (Jeanloz and Knittle, 1989; Ricolleau et al., 2009).

We introduce the notion of "maximum Al uptake capacity" of perovskite. "Maximum Al uptake capacity" conditions are set through a *virtual* competition between $MgSiO_3$ and $Al_2O_3$ (ideal *pure* alumina phase) to accommodate Al, at lower mantle *P-T* conditions and in a $SiO_2$-MgO-$Al_2O_3$ system. Corundum (*cor*) is the least "prejudicial" phase as an Al host, given that it does not require any further chemical species but aluminium to form and is the $Al_2O_3$-polymorph stable in the *P-T* range of interest (Merli and Pavese, 2018).

The incorporation mechanism of a trivalent cation in perovskite is supposed to occur through three main reactions (Navrotsky et al., 2003; Akber-Knutson et al., 2005 and references therein):

(i) $Si^{4+} + Mg^{2+} = M^{3+} + M^{3+}$
(ii) $Si^{4+} = M^{3+} + 1/2\ V_O^0$
(iii) $Si^{4+} = M^{3+} + H^+$.

Reaction (i), which takes place *via* a charge-coupled-mechanism, is the likeliest one, as shown by energy calculations (Yamamoto et al., 2003; Akber-Knutson et al., 2005; Zhang and Oganov, 2006). A comparison between incorporation mechanisms (i) and (ii) reveals that the former is slightly exothermic, in contrast with the endothermic behaviour of the latter (Navrotsky et al., 2003). NMR measurements point to the occurrence of a charge-coupled mechanism (Stebbins et al., 2001), in agreement with calculations of Akber-Knutson and Bukowinski (2004), who suggest that Al tends to replace both Si and $M^{2+}$, in a high pressure and high temperature regime. As to reaction (iii), we assume contents of $H_2O$, *i.e.* $H^+$ supplier, and $Al_2O_3$ as much as 1500 ppm (0.15 wt%) and 4.76 wt%, respectively (Table 1), in keeping with the lower mantle Al richest composition obtained by mixing pyrolite with 3% MORB component (Table 1). In such a case, even if all the hydrogen from the dissociation $OH_2 \rightarrow OH^- + H^+$ contributed to an exchange mechanism like (iii), just 0.08 mol fraction aluminium might be accounted for. Moreover, according to the $H_2O$ partitioning estimated by Merli et al. (2016), periclase is able to account for 1/3 of the trapped $H_2O$, thus reducing further the role of reaction (iii) as a possible relevant mechanism to Al incorporation in perovskite.

Therefore, the Al uptake in perovskite is modelled by the replacement of Mg-Si with Al-Al, according to the exchange reaction reported below using the formalism of Kröger-Vink (Kröger, 1972)

$$Al_2O_3 + [Mg_{Mg}]^X + [Si_{Si}]^X \quad [Al_{Mg}]^{'} + [Al_{Si}]^{'} + MgSiO_3. \tag{4}$$

Assuming λ-mole of $Al_2O_3$ to be exchanged in the *Mg-Al-pv*, *Mg-pv* and *cor* system, then Eq. (4) leads to

$$(1-\lambda)MgSiO_3 + \lambda Al_2O_3 \iff (Mg_{1-\lambda}Al_\lambda)(Si_{1-\lambda}Al_\lambda)O_3. \tag{5}$$

In reaction (5) iron can affect the energy through a replacement like $Mg^{2+} \Leftrightarrow Fe^{2+}$ and competes with aluminium in terms of $Al^{3+} \Leftrightarrow Fe^{3+}$. However, we chose to neglect Fe as we are developing a first approximation model, which would provide general trends rather than details. Our choice can be further supported by the following arguments.

- The general reaction that accounts for $Al_2O_3$ entering in bridgmanite turns out to be

$$\begin{aligned}&(Mg_{1-x}Fe_x^{2+})SiO_3 + \lambda Al_2O_3 \\ &= \left(Mg_{1-x-\lambda/2}Fe_{x-\lambda/2}^{2+}Al_\lambda\right)(Si_{1-\lambda}Al_\lambda)O_3 \\ &\quad + \lambda\left(Mg_{\frac{1}{2}}Fe_{\frac{1}{2}}^{2+}\right)SiO_3\end{aligned} \tag{6}$$

where we assume that Al replaces the same quantity of Mg and $Fe^{2+}$, the latter dwelling at the 12-coordination site, only (Kaminsky and Lin, 2017). The parametrization of the Gibbs energy used in the present work relies upon the cluster expansion technique (Merli et al., 2015; 2017). Such a method leads to expressing energy as a function of the number of interacting atomic pairs that belong to the same cluster determined as a function of the distance between the involved chemical species. Assuming Fe-Al pair entering the perovskite structure as much as 0.1–0.2 moles (*i.e.* Kurnosov et al., 2017; Kaminsky and Lin, 2017), the probability of having a Fe-Al interacting pair belonging to the first/second cluster is ~5–6%. Therefore, most of the interactions with aluminium atoms are due to the pure Mg-Si matrix, which governs the "maximum intrinsic capacity" of perovskite to incorporate Al.

The role of $Fe^{3+}$ is extensively debated and still largely uncertain. *Mg-Fe-pv* is potentially the major $Fe^{3+}$ acceptor, but Kaminsky and Lin (2017) indicated that in natural lower mantle bridgmanites, iron most likely occurs as ferrous at the 12-coordination sites. Conversely, Kurnosov et al. (2017) claim $Fe^{3+}/\Sigma Fe_{tot} = 0.33$, in synthetic bridgmanite with ferric iron sited at the same coordination site,

under lower mantle conditions ($P \sim 35$ GPa; 1300 km depth; Ismailova et al. 2016). Mass balance calculations, in turn, predict an impact of ferric iron in terms of $Fe^{3+}/\sum Fe_{tot} \sim 0.03$, with respect to the Earth's mantle abundances (Palme and O'Neill, 2014). If we consider as a first level of approximation pyrolite (*Mg-Fe-pv* = 76 wt %; $FeO_{tot} = 8.05$ wt%) and chondrite (*Mg-Fe-pv* = 85 wt %; $FeO_{tot} = 8.12$ wt%) lower mantle models (Table 1), and apply the Kurnosov et al. (2017) $Fe^{3+}/Fe_{tot}$ ratio to *Mg-Fe-pv*, the resulting $Al^{3+}/Fe^{3+}$ mole ratios in bridgmanite are ~3.6 and ~2.9 for pyrolite and chondrite models, respectively. Tests based on calculations that we carried out to reproduce the replacement schemes $Si + Mg \Leftrightarrow Al + Fe^{3+}$ *versus* $Si + Mg \Leftrightarrow Al + Al$, indicate that the second reaction is favoured over the former one [in agreement with the results of Nishio-Hamane et al. (2005)].

### 3.3. Reaction models

The Al uptake mechanism in perovskite according to reaction (5) is addressed using two approaches: (i) the *open system model*, which exploits the notion of the stationary thermodynamic state and allows an exchange of matter between system and reservoir (Prigogine, 1968); (ii) the *closed system model*, which relies on equilibrium thermodynamics, therefore excluding any sort of matter exchange. In an open system, the stationary state replaces the equilibrium state and exhibits thermodynamic observables, which remain invariant over time. Details about the open system model are reported in Appendix A.1–A.3 and a brief overview is given below.

#### 3.3.1. Open system model

We would like to exploit the capacity of an open system to exchange matter with a reservoir, in combination with a formalism as close as possible to the consolidated equilibrium thermodynamics' one. Such a model provides a flexible tool to address problems in which the intrinsic exchanging/incorporation capacity of a given substance can be investigated, without any sort of constraint or restraint (Appendx A.1).

The key requirement is the fulfilment of the following equation, associated to reaction (5) *via* the equilibrium constant $K$ (Appendix A.2 and A.3):

$$K(P,T,\lambda) = exp[-\Delta G_0(P,T,\lambda)/RT] = a_{Mg-Al-pv}/\left(a_{Mg-pv}^{1-\lambda} \times a_{cor}^{\lambda}\right) \approx x_{Mg-Al-pv}/\left(x_{Mg-pv}^{1-\lambda} \times x_{cor}^{\lambda}\right) \quad (7.a)$$

where $x_j$ = phase proportion of the $j^{th}$ component/phase (*cor*: corundum); $a_j = j^{th}$ component/phase's activity. In Eq. (7.a) the activity coefficient is approximated to unity (see Appendix A.3 and B). Expanding $\Delta G_0$, it follows that:

$$\Delta G_0(P,T,\lambda) = \mu_0(P,T,\lambda)_{Mg-Al-pv} - \lambda \times \left[\mu_0(P,T)_{cor} - \mu_0(P,T)_{Mg-pv}\right] - \mu_0(P,T)_{Mg-pv} \quad (7.b)$$

where $\mu_0$ is the part of the chemical potential depending on $\lambda$, $P$ and $T$, only (Ottonello, 1997, 2010). For convenience, we split the chemical potential of Al incorporating perovskite (*Mg-Al-pv*) into an Al free part, *i.e.* pure perovskite (*Mg-pv*), and a part dependent on aluminium, that is

$$\mu_0(P,T,\lambda)_{Mg-Al-pv} = \mu_0(P,T)_{Mg-pv} + \Delta\mu_0(P,T,\lambda)_{Mg-Al-pv} \quad (7.c)$$

where $\Delta\mu_0(P, T, \lambda)_{Mg\text{-}Al\text{-}pv}$, which accounts for the solid mixing occurrence and provides the very core of our computational model, is calculated by the cluster expansion method (Merli et al., 2015, 2017).

Using Eqs. (7.c) and (7.b) becomes

$$\Delta G_0(P,T,\lambda) = \Delta\mu_0(P,T,\lambda)_{Mg-Al-pv} - \lambda\left[\mu_0(P,T)_{cor} - \mu_0(P,T)_{Mg-pv}\right] \quad (8)$$

At given ($P$, $T$, $\lambda$)-values, we seek the $\{x_{Mg\text{-}Al\text{-}pv}, x_{Mg\text{-}pv}, x_{cor}\}$-sets that fulfil

a) Eq. (7.a),
b) $x_{Mg\text{-}Al\text{-}pv}, x_{Mg\text{-}pv}, x_{cor} \geq 0$,
c) $x_{Mg\text{-}Al\text{-}pv} + x_{Mg\text{-}pv} + x_{cor} = 1$.

Among the solutions that satisfy the constraints (a), (b) and (c), we chose the one that minimizes the Gibbs energy, namely $x_{Mg\text{-}Al\text{-}pv} \times \mu_0(P, T, \lambda)_{Mg\text{-}Al\text{-}pv} + x_{Mg\text{-}pv} \times \mu_0(P,T)_{Mg\text{-}pv} + x_{cor} \times \mu_0(P,T)_{cor}$. In doing so, we obtain a triple, yielding *Mg-Al-pv*/*Mg-pv*/*cor* phase proportions, for each ($P$, $T$, $\lambda$) point, *i.e.* $\{x_{Mg\text{-}Al\text{-}pv}, x_{Mg\text{-}pv}, x_{cor}\}(P, T, \lambda)$. The preservation of the total chemical composition of the system constituted by each $\{x_{Mg\text{-}Al\text{-}pv}, x_{Mg\text{-}pv}, x_{cor}\}(P, T, \lambda)$-triple is not required. The resulting system therefore behaves as an open system that can exchange $2Al \Leftrightarrow Mg + Si$ with a reservoir. In general, we are interested in modelling *observables* whose values are averages over the $\lambda$-range, so that they depend ultimately on $P$-$T$ only. For instance:

$$\left\{x_{Mg-Al-pv}, x_{Mg-pv}, x_{cor}\right\}(P,T) = \frac{1}{C}\int_{\lambda-inf}^{\lambda-sup}\left\{x_{Mg-Al-pv}, x_{Mg-pv}, x_{cor}\right\}(P,T,\lambda)\mathrm{d}\lambda \quad (9.a)$$

$$\lambda_{Al2O3}(P,T) = \int_{\lambda-inf}^{\lambda-sup}\lambda \times x_{Mg-Al-pv}(P,T,\lambda)\mathrm{d}\lambda / x_{Mg-Al-pv}(P,T) \quad (9.b)$$

$$Tot_{Al2O3}(P,T) = \frac{1}{C} \times \int_{\lambda-inf}^{\lambda-sup}\left[\lambda \times x_{Mg-Al-pv}(P,T,\lambda) + x_{Al2O3}(P,T,\lambda)\right]\mathrm{d}\lambda \quad (9.c)$$

where: C is a normalization constant; $\lambda$-sup = 0.3 and $\lambda$-inf = 0, upper and lower thresholds of $\lambda$, respectively (for $\lambda > 0.3$, $x_{Mg\text{-}Al\text{-}pv}$ is negligible on the $P$-$T$ range explored); $\lambda_{Al2O3}$ of (9.b) is the *average* $Al_2O_3$ mole fraction *per* formula unit; $Tot_{Al2O3}$ is the total $Al_2O_3$ stored by the (*Mg-Al-pv*)+(*Mg-pv*) + *cor* system.

*3.3.2. Closed system model*

For the sake of completeness, we also present the closed system model. We seek the equilibrium conditions of reaction (5) for a closed system, *i.e.* chemically adiabatic. Let ξ represent the aluminium occupancy factor in *Mg-Al-pv* [*i.e.* $(Mg_{1-\xi}Al_{\xi})(Si_{1-\xi}Al_{\xi})O_3$]. Therefore, we have to minimize, with respect to ξ, the Gibbs energy of the system (*Mg-pv*) + (*Mg-Al-pv*) + *cor*, *i.e.*

$$G = n_{cor} \times \mu_0(P,T)_{cor} + n_{pv} \times \mu_0(P,T)_{Mg-pv} + n_{Mg-Al-pv} \times \mu_0(P,T,\xi)_{Mg-Al-pv} \quad (10)$$

under the constraints of the conservation of mass:

$$M_{Al2O3} = n_{cor} + n_{Mg-Al-pv} \times \xi \quad (11)$$

$$M = M_{SiO2} = M_{MgO} = n_{Mg-pv} + n_{Mg-Al-pv} \times (1-\xi), \quad (12)$$

where $M_{Al2O3}$, $M_{SiO2}$ and $M_{MgO}$ are *fixed* total amounts in moles of $Al_2O_3$, $SiO_2$ and MgO.

Using the constraints above, Eq. (10) becomes

$$G = \left(M_{Al2O3} - n_{Mg-Al-pv} \times \xi\right) \times \mu_0(P,T)_{cor} + \left(M - n_{Mg-Al-pv} \times (1-\xi)\right) \times \mu_0(P,T)_{Mg-pv} + n_{Mg-Al-pv} \times \mu_0(P,T,\xi)_{Mg-Al-pv} \quad (13)$$

The Gibbs energy minimum condition requires

$$\frac{\partial G}{\partial \xi} = 0,$$

from which the following equation is derived

$$-\mu_0(P,T)_{cor} + \mu_0(P,T)_{Mg-pv} + \frac{\partial \mu_0(P,T,\xi)_{Mg-Al-pv}}{\partial \xi} = 0. \quad (14)$$

Eq. (14) formalises the equilibrium conditions for closed systems (Chust et al., 2017). Its solution, expressed by $\xi_{closed\ system}$, yields the composition of Al bearing perovskite that minimises the Gibbs energy of Eq. (13).

$\xi_{closed\ system}$ also minimises (7.b). In fact, taking into account Eq. (7.c) and (14) is equivalent to setting $\frac{\partial \Delta G_0(P,T,\lambda)}{\partial \lambda} = 0$ in Eq. (8), which implies that $K(P,T,\xi_{closed\ system})$ achieves an extreme value that shifts reaction (5) towards its right-hand side member as much as possible.

### 3.4. Computational

Structure relaxations were performed at a given pressure and 0 K by the HF/DFT-CRYSTAL14 program (Dovesi et al., 2009), which implements "A*b-initio* Linear-Combination-of-Atomic-Orbitals" for periodic systems. Only static pressure ($P_{static} = -\partial E_{static\ energy}/\partial V$) and zero-point pressure ($P_{zp} == -\partial E_{vibration\ energy\ at\ 0K}/\partial V$) were taken into account, given that adding a correction for thermal contributions would not significantly change our results and the conclusions would be unaffected. A zero-point pressure was estimated by quantum mechanics calculations and using *pure perovskite* only, resulting in ~5 GPa. The WCGGA functional (Wu and Cohen, 2006) was used, with a hybridization rate of 28%. Such a proportion was adopted because it provides a more satisfactory agreement with observations in terms of perovskite structure, than other choices do. The tolerances governing the accuracy of the integrals of the self-consistent-field-cycles were set at (in Ha units): $10^{-8}$ for coulomb overlap, $10^{-8}$ for coulomb penetration, $10^{-8}$ for exchange overlap, $10^{-8}$ for exchange pseudo-overlap in direct space, $10^{-16}$ for exchange pseudo-overlap in reciprocal space and $10^{-9}$ for threshold for SCF-cycles' convergence. The Mg basis set from Causà et al. (1986) was extended by the addition of diffuse *sp* and *d* shells (85-11G* contraction). Oxygen and aluminium were modelled by means of the O8-411d1 and 85-11G* basis sets of Corà (2005) and Catti et al. (1994), respectively. The outer shells' coefficients were optimised by means of the "billy" utility by Towler (2015). The eigenvalue level shifting technique was used (level shift of 0.2 Ha) to avoid conducting solutions and accelerate convergence.

The approach of Merli et al. (2015 and 2017) relying upon the cluster expansion technique was adopted to model the solid mixing in *Mg-Al-pv*. Such a method makes it possible to parametrize energy as a function of pair interactions, thus allowing one to model in a statistical framework even large atom clusters that would be difficult to handle otherwise. We expressed the Al dependent part of the chemical potentials in Eq. (7.b) as

$$\Delta\mu_0(P,T,\lambda)_{Mg-Al-pv} = \mu_0(P,T,\lambda)_{Mg-Al-pv} - \mu_0(P,T)_{pv} = \lambda \times \left[\mu_0(P,T,\lambda)_{Mg-Al-pv} - \mu_0(P,T)_{cor}\right] + \delta\mu_0(P,T,\lambda)_{Mg-Al-pv} \quad (15)$$

$\delta\mu_0(P, T, \lambda)$, in turn, was developed in terms of

$$\delta\mu_0(P,T,\lambda)_{Mg-Al-pv} = (1-\lambda) \times \lambda \times \sum\nolimits_{l=0,L;m=0,M;n=0,N} p_{lmn} P^l T^m \lambda^n \quad (16)$$

We used perovskite's supercells, composed of (2 × 2 × 1), (2 × 1 × 2) and (1 × 2 × 2) elementary cells. A total of 80 independent Al configurations were randomly sampled over the interval 24–80 GPa and used to calculate the pair-interaction parameters of the cluster expansion as a function of *P*, following the strategy of Merli et al. (2017). We then simulated $10^5$-$10^6$ *Mg-Al-pv* independent configurations in 1024 atom clusters, using the pair-interaction parameters previously determined, to carry out statistical thermodynamic calculations (Merli et al. 2015), and model the Gibbs energy of Al bearing perovskite thereby.

$\Delta G_0$ in Eq. (7.b) were calculated neglecting the atomic vibration contribution, *i.e.* the one including zero-point vibration energy, thermal vibration energy and vibration entropy (in full: $\Delta G_{0,vib}$). In general, calculating $\Delta G_{0,vib}$ in a solid mixing that is modelled *via* a super-cell method is a difficult task, because of the complexity of compromising among representativeness of a cluster, computing time, and achievable precision (about the role of vibrational components, see: van de Walle and Ceder, 2002). However, combining quantum calculations with semi-empirical potentials (GULP code; Gale, 1997, 2005), which allow the investigation of large atomic clusters' lattice dynamics, we estimated by harmonic approximation, $\Delta G_{0,vib}$ for 4 Al-Al configurations in perovskite at 20 and 70 GPa, with 0.25 $Al_2O_3$ mole fraction. In this way we compared $\Delta G_{0,vib}$ with $\Delta G_{0,stat+conf}$,

Table 3
*Chemical probability of formation* [*p*(J,chem)] expressed in % of potential lower mantle Al bearing phases.

| | | Pyrolite | | Chondrite | |
|---|---|---|---|---|---|
| **Phase name** | **Composition** | **A** | **A + 3%B** | **A1** | **A1 + 3%B** |
| Mg-Al-perovskite | $(Mg_{0.9}Al_{0.1})(Si_{0.9}Al_{0.1})O_3$ | 96.04 | 95.63 | 96.39 | 95.98 |
| δ-phase[1] | AlO(OH) | 0.25 | 0.27 | 0.20 | 0.23 |
| H-phase[2] | $(MgSi,Al_2)O_4H_2$ | 0.21 | 0.22 | 0.20 | 0.21 |
| D-phase[3] | $Al_2SiO_4(OH)_2$ | 0.01 | 0.01 | 0.01 | 0.01 |
| NAL/CF[4] | $Na_{0.265}Fe_{0.245}Mg_{0.375}Ca_{0.035}Al_{1.1}Si_{0.715}O_4$ | 3.50 | 3.87 | 3.20 | 3.57 |
| | | 100.00 | 100.00 | 100.00 | 100.00 |

End-member A from McDonough and Sun (1995).
End-member A1 from Merli et al. (2016), modified.
End-member B = MORB-like silicate glass of Hirose et al. (1999).
[1] Ohtani et al. (2001).
[2] Ohtani et al. (2014).
[3] Pamato et al. (2015).
[4] Guignot and Andrault (2004).

*i.e.* the static contribution with the addition of configuration entropy, which we calculated. We observed $|\Delta G_{0,vib}/\Delta G_{0,stat+conf}| \sim 3\%$, in the thermal range of interest, *i.e.* 2000–3000 K. Therefore, considering the modest estimated weight of the thermal contribution in the solid mixing, we chose to exclude it (as for neglecting vibration contribution, see for instance: Mohn and Trønnes, 2016; Burton and van de Walle, 2003).

## 4. RESULTS

### 4.1. Chemical probability of formation of lower mantle phases

The largest bulk aluminium content of a *non-primitive* lower mantle (4.76 wt% related to the pyrolite mixed with 3% of crustal component) along with the available amounts of alkali elements and $H_2O$ make the *chemical probability of formation* [*p*(J,chem)] for the minor Al bearing phases < 0.9% (Table 1; Table 2). As expected, the *p*(J,chem) of *Mg-Fe-pv* + *Mg-pv* + *Ca-pv* + *Fe-pe* in a *non-primitive* lower mantle is >78%, regardless of the geochemical model used. It is worth noting that *p*(J,chem) of *Mg-Al-pv* is as large as ~96%, considering the Al bearing phases only (Table 3). The hydrous phases are *quasi* irrelevant, whereas the NAL/CF type phase exhibits a *p*(J,chem) as large as 3.87–3.57% (Table 3).

If we used *p*(J,chem) as an "actual" *probability of finding a given phase*, then Al would distribute in terms of 4/5 *versus* 1/5 between *Mg-Al-pv* and *CF* (the CF phase is able to host almost six times as much aluminium as perovskite). This estimate is to be taken with due care as *p*(*Mg-Al-pv*,chem) and *p*(*CF*,chem) quantify only the probability of having the "least condition" for a given phase to form, regardless of the energy contribution and inter-phase competition to capture the involved elements. Altogether, perovskite is the main candidate to incorporate aluminium by far, though *CF* also exhibits a potential capacity for Al storing.

### 4.2. Al uptake in perovskite: open system model *versus* closed system model

The main advantages of using an *open system model* with respect to a *closed system model* are the following:

- neglecting the chemical composition invariance allows the system to evolve *unconstrained*, driven by the mixing Gibbs energy of the solid solution of *Mg-Al-pv*. This provides the most favourable condition to estimate the *Mg-Al-pv*'s intrinsic maximum capacity to host Al, resorting to a simple system composed of perovskite in combination with free alumina (*cor*), the latter accounting for the aluminium not incorporated by the former because of saturation;
- such a method makes it possible i) to achieve an average depiction of the output of a given chemical process and ii) to explore a mechanism of Al storage taking into account not only the Al occupancy in perovskite, but also the amount of perovskite that is able to host aluminium *versus* the fraction of Al free perovskite (*Mg-Al-pv*/*Mg-pv*).

Reaction (5) was investigated using the *P-T* curve parametrised by Merli et al. (2016) as follows

$$T(\mathrm{K}) = 11.290 \times P(\mathrm{GPa}) + 1648,$$

for $24 < P < 80$ (GPa). Such a curve represents a lower mantle in a whole mantle convention of limited thermal efficiency (Mattern et al., 2005; Stixrude and Lithgrow-Bertelloni, 2005), thus approaching the layered mantle convection models (Brown and Shankland, 1981; Anderson, 1989; Valencia-Cardona et al., 2017).

#### *4.2.1. Al uptake in perovskite from open system model*

Fig. 1 shows $K(P, T, \lambda)$ of Eq. (7.a) as a function of λ, at three chosen *P-T* points. In general, the larger the value of *K*, the more reaction (5) shifts to the right, *i.e.* towards *Mg-*

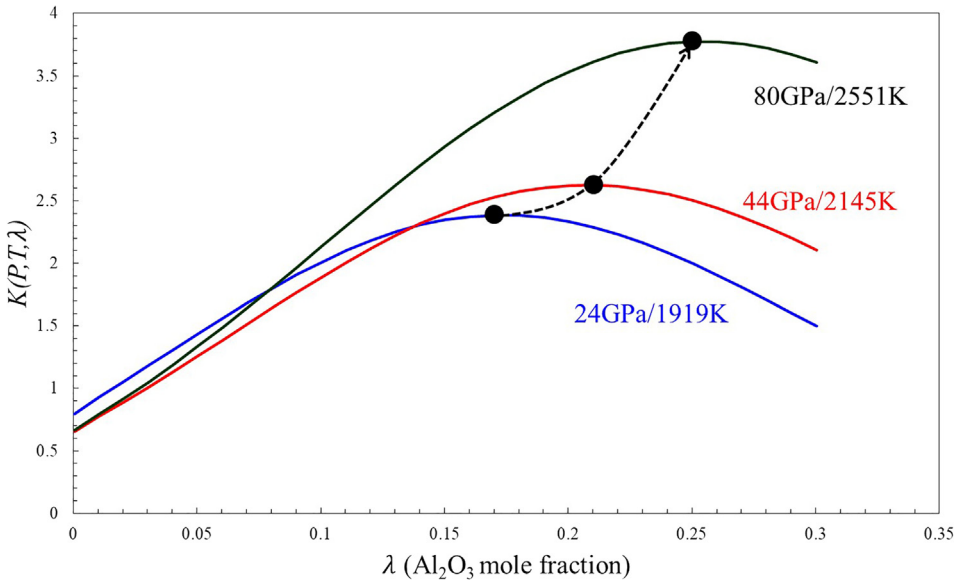


Fig. 1. Equilibrium constant, $K(P, T, \lambda)$, of the fundamental alumina exchange reaction (5) *versus* λ, which expresses the exchanged amount of $Al_2O_3$ in the *Mg-Al-pv*, *Mg-pv* and *cor* system. $K(P, T, \lambda)$, calculated by the open system model, is displayed at 24 GPa/1919 K (blue line), 44 GPa/2145 K (red line) and 80 GPa/2551 K (black line), by way of example. Black filled circles indicate the maxima at the three chosen *P-T* points, and correspond to the λ-values that most shift the reaction (1-λ) $MgSiO_3 + \lambda\ Al_2O_3 \leftrightarrow (Mg_{1-\lambda}Al_\lambda)(Si_{1-\lambda}Al_\lambda)O_3$ to the right (Eq. (5), of the text).

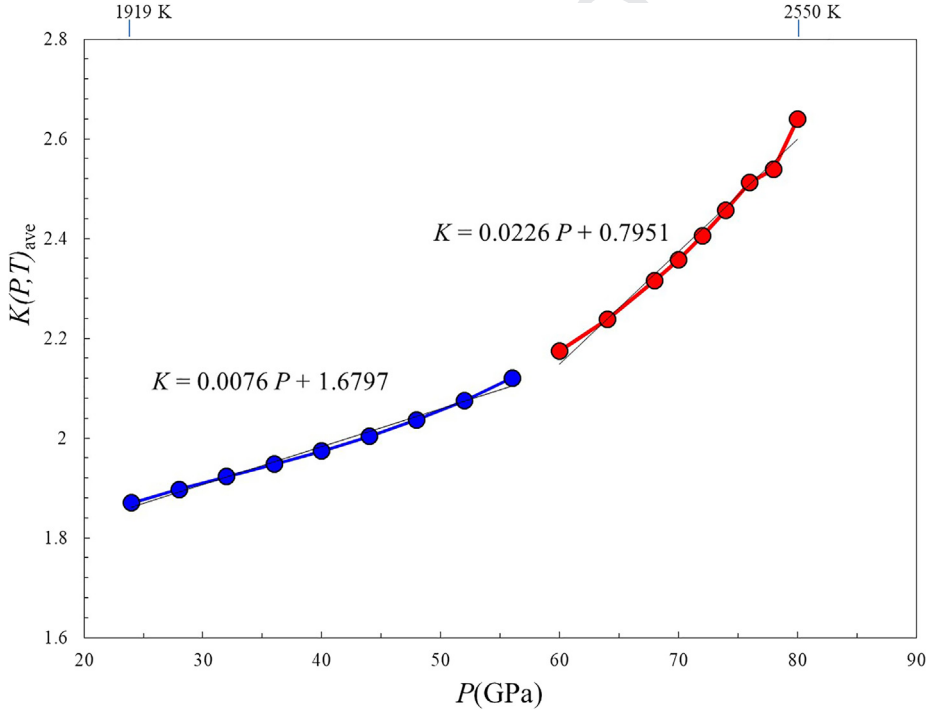


Fig. 2. $K(P,T)_{ave}$ *versus* *P*, according to the chosen geotherm and calculated by the open system model. Blue line and red line show two different trends for the average equilibrium constant, $K(P,T)_{ave}$, of the reaction (5). Note that $K(P,T)_{ave} = \langle K(P, T, \lambda)\rangle_\lambda$ (see 4.2.1 section for further explanations).

*Al-pv*. For each *P-T* point, $K(P, T, \lambda)$ has a maximum that changes from about 0.17 (24 GPa/1919 K) to 0.26 (80 GPa/2551 K). This means that there is an Al exchange λ-value that maximises the tendency to promote *Mg-Al-pv* at each *P-T* point of the geotherm. We now introduce the function $K(P,T)_{ave}$, which corresponds to the average of the equilibrium constant of reaction (5), *i.e.* $K(P,T)_{ave} = <K(P, T, \lambda)>_\lambda$. $K(P,T)_{ave}$ provides an overview of the general

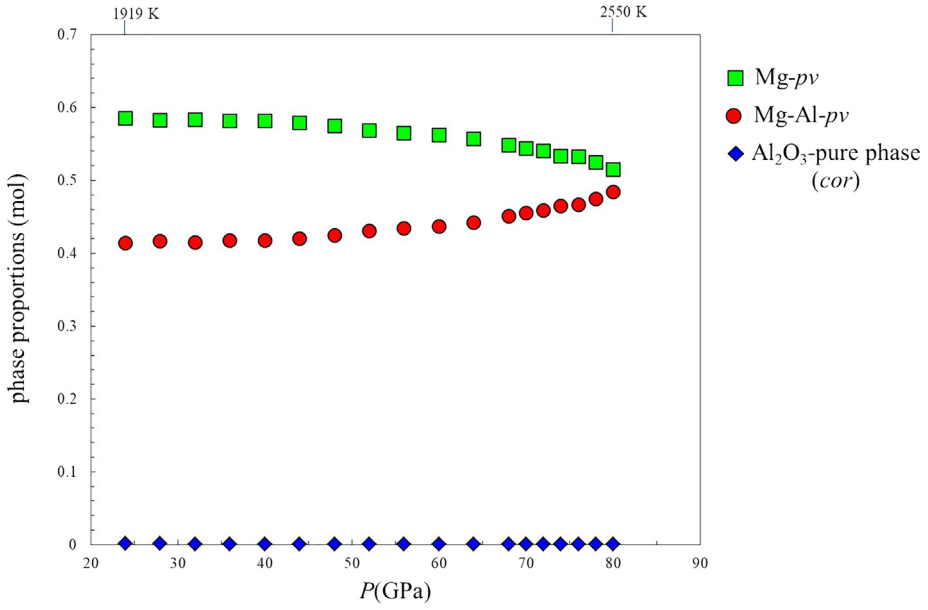


Fig. 3. Phase proportions of Al free perovskite (*Mg-pv*), Al bearing perovskite (*Mg-Al-pv*) and corundum (*cor*) *versus* *P*, according to the chosen geotherm. *Mg-Al-pv* fractions have an average $Al_2O_3$ composition provided by $\lambda_{Al2O3}$, calculated according to Eq. (9.b) on the *P-T* range of interest and shown in Fig. 5. Al free perovskite is an extreme notion, which provides a "limit" to define a tendency of such mineral to incorporate aluminium.

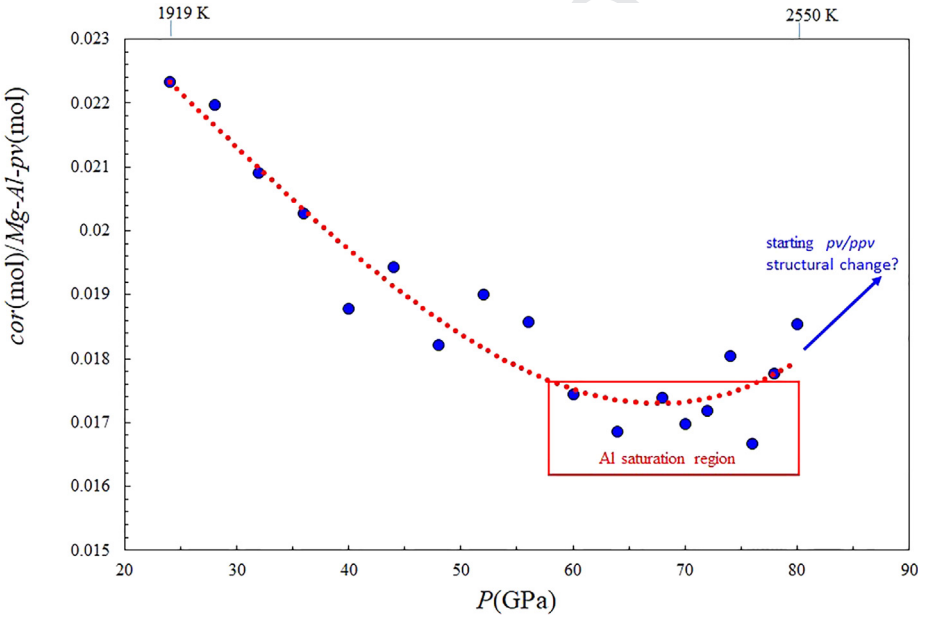


Fig. 4. $Al_2O_3$ partitioning between corundum and perovskite (*cor*(mol)/*Mg-Al-pv*(mol)) *versus* *P*, according to the chosen geotherm and calculated by the open system model. The red box shows the region of maximum Al uptake for perovskite (saturation region), suggesting that at such *P-T* conditions the Al incorporation is weakly dependent on pressure. At higher pressure, the *cor*/*Mg-Al-pv* ratio trend hints at a possible instability of perovskite (transition to another phase, such as post perovskite, *ppv*?). See text for further discussion.

tendency of the aluminium incorporation process to shift either to the right or left in reaction (5) along the chosen *P-T* path (Fig. 2). $K(P,T)_{ave}$ calculated over Al exchange processes between corundum and perovskite from 0 to 0.3 λ-value, tends to increase upon increasing *P*, *i.e.* reaction (5) shifts more and more to its right-hand side member $[(Mg_{1-\lambda}Al_{\lambda})(Si_{1-\lambda}Al_{\lambda})O_3]$. Two trends of $K(P,T)_{ave}$ are observable: one below and one above ~60 GPa, characterised by 0.008 and 0.02 $GPa^{-1}$ slopes, respectively (Fig. 2). They are reflective of the growing differences between the $K(P, T, \lambda)$-curves, for $\lambda > 0.15$ (Fig. 1). On the explored *P-T* interval, the content of free $Al_2O_3$, *i.e.*

Please cite this article in press as: Merli M., et al. Aluminium distribution in an Earth's *non–primitive* lower mantle. *Geochim. Cosmochim. Acta* (2020), https://doi.org/10.1016/j.gca.2020.02.023

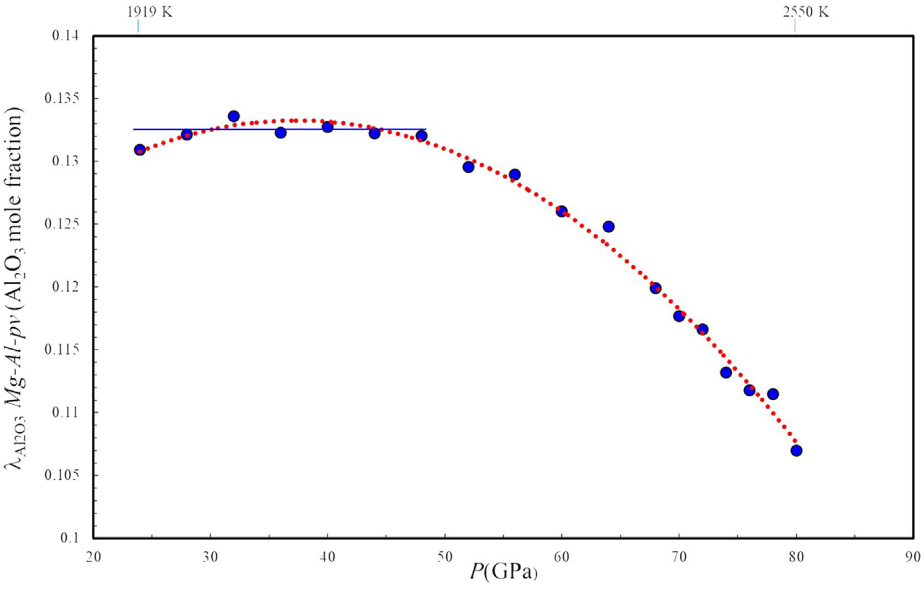


Fig. 5. Average $Al_2O_3$ mole fraction in perovskite, $\lambda_{Al2O3}$, determined by the open system model and calculated *via* Eq. (9.b), as a function of $P$ along the chosen geotherm. In the $P$-region 30–50 GPa, $\lambda_{Al2O3}$ is *quasi* constant (interpolation solid line).

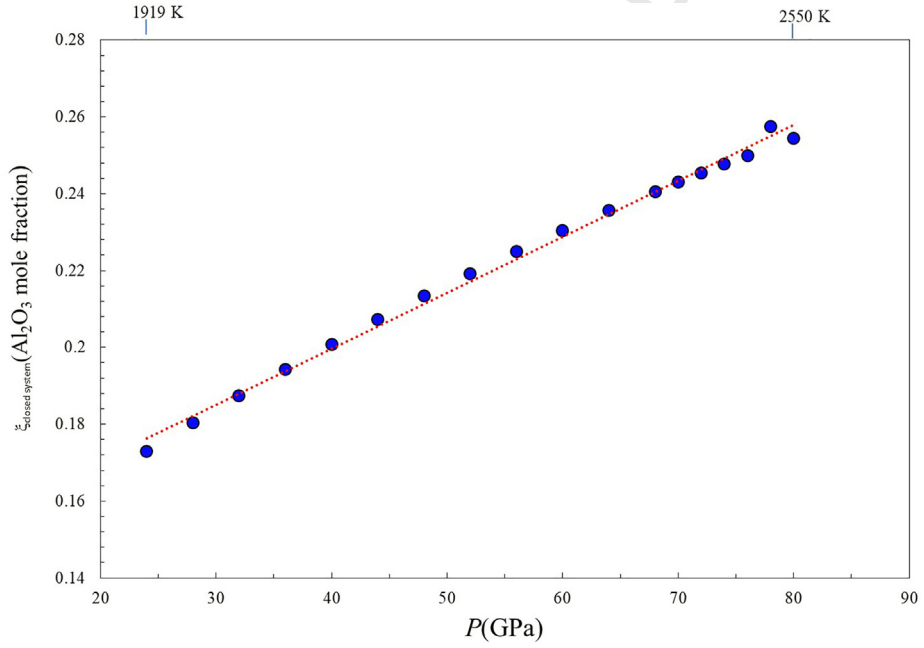


Fig. 6. $Al_2O_3$ mole fraction in perovskite, $\xi_{closed\ system}$, determined by the closed system model and calculated *via* Eq. (14), as a function of $P$ along the chosen geotherm. At $\lambda = \xi_{closed\ system}$, $K(P, T, \lambda)$ takes an extreme value, so that reaction (5) is shifted to the right as much as possible.

*cor*, takes a very small average figure of 0.0010(±1), in terms of phase proportion. Conversely, Al free (*Mg-pv*) and Al bearing (*Mg-Al-pv*) perovskite phases amount to 0.56(±2) and 0.44(±2), respectively (Fig. 3). *Mg-Al-pv* increases from 0.41 to 0.48 phase proportion, from 24 to 80 GPa: this hints at a tendency to develop increasingly more (Mg,Al)(Si,Al)$O_3$-phase upon $P$ (Fig. 3).

The *cor*/*Mg-Al-pv* ratio monotonically decreases with increasing pressure up to 70 GPa (Fig. 4), from more than 0.022 to about 0.017, meaning that some 98 wt% of available $Al_2O_3$ is taken by perovskite, in agreement with the results shown in Figs. 1–3. In the range 60–80 GPa the data are rather scattered and weakly $P$-dependent. They indicate either some sort of "saturation" (with respect to perovskite) or a poorly defined minimum. The aluminium uptake capacity of perovskite is described *via* $\lambda_{Al2O3}$, see Eq. (9.b), that gives the average $Al_2O_3$ mole fraction *per* formula unit (Fig. 5). At 32 GPa perovskite hosts $Al_2O_3$ at its max-

Please cite this article in press as: Merli M., et al. Aluminium distribution in an Earth's *non–primitive* lower mantle. *Geochim. Cosmochim. Acta* (2020), https://doi.org/10.1016/j.gca.2020.02.023

imum capacity ($\lambda_{Al2O3} = 0.134$ $Al_2O_3$ mole fraction) and preserves such an occupancy figure up to ~50 GPa (Fig. 5). The occupancy starts to monotonically decrease beyond 50 GPa, with a slope of about $-0.0009$ $GPa^{-1}$ ($\lambda_{Al2O3} = 0.105$ $Al_2O_3$ mole fraction, at 80 GPa; Fig. 5). This takes place in combination with an increase of the phase fraction of Al bearing perovskite.

#### 4.2.2. Al uptake in perovskite from a closed system model

The Al occupancy factor $\xi_{closed\ system}$, as reported in Eqs. (10)–(12), minimises the Gibbs energy and maximises the equilibrium constant of Eq. (7.a), *i.e.* if $\lambda = \xi_{closed\ system}$ then $K(P, T, \lambda)$ takes its maximum value. $\xi_{closed\ system}$ exhibits a linear and increasing trend, trailing down the mantle (Fig. 6). This implies that the perovskite structure incorporates increasingly more aluminium as the pressure increases, if the system is *chemically adiabatic* and *cor* only competes to host Al. Such a result can be seen if a given amount of Al must be "*perforce*" accommodated over perovskite and *cor*, then aluminium chooses progressively the former with respect to the latter with increasing $P$, thus yielding a shift of reaction (5) to the right.

### 4.3. Solid mixing model performances with respect to some experimental data

We tested the physical soundness of our mixing energy model comparing its predictions with some experimental results related to *Mg-Al-pv* properties.

The enthalpy formation of the reaction 0.05 $Al_2O_3$ (*cor*) + 0.95 $MgSiO_3 = Mg_{0.9}Si_{0.9}Al_{0.1}O_3$ was measured to be as large as $-0.8(\pm 2.2)$ kJ/mol by Navrotsky et al. (2003). Such a figure is to be compared with $-1.1$ kJ/mol from our calculations. Although our estimation is 40% larger than the experimental value, the exothermic nature of the reaction is correctly predicted and, considering the uncertainty of measurements, observation and theoretical estimate are in good agreement. In Fig. 7, we report the absolute values of the discrepancy between measurements (Walter et al., 2004) and our predictions on the Al bearing perovskite cell volume. In most cases, the deviation lies below 0.8%, and just for three experimental points we observe a discrepancy above 1%. Altogether, the average disagreement is about 0.4% and indicates a chemical-physical soundness of the solid mixing model we are using.

## 5. DISCUSSION

### 5.1. Aluminium storage mechanism

Our results from the open system model point to a complex mechanism of Al uptake in perovskite as a function of pressure (Figs. 3–5). In particular, the aluminium storage involves both the *Mg-Al-pv* phase proportion and the average $Al_2O_3$-mole fraction incorporated by *Mg-Al-pv* (*i.e.* $\lambda_{Al2O3}$; see equ.(9.b)). Whereas $\lambda_{Al2O3}$ (Fig. 5) changes comparably little and, in general, moderately decreases at large pressures, the phase fraction of *Mg-Al-pv* grows by ~16% upon increasing $P$ (Fig. 3).

We underline that our model relies on mass transfer reactions within a chemically unconstrained open system constituted by *Mg-pv* + *Mg-Al-pv* + *cor* that act as Al-Mg-Si exchangers with an ideal reservoir; therefore, the calculated maximum Al uptake capacity in perovskite is independent of the geochemical frame.

A lower mantle composition with chondritic Mg/Si ratio of ~1.01 implies an amount of perovskite from 83 up to 90 wt%, juxtaposed to the pyrolitic composition that predicts perovskite in the narrow range of 75–78 wt% (Lyubetskaya and Korenaga, 2007, McDonough, 2016).

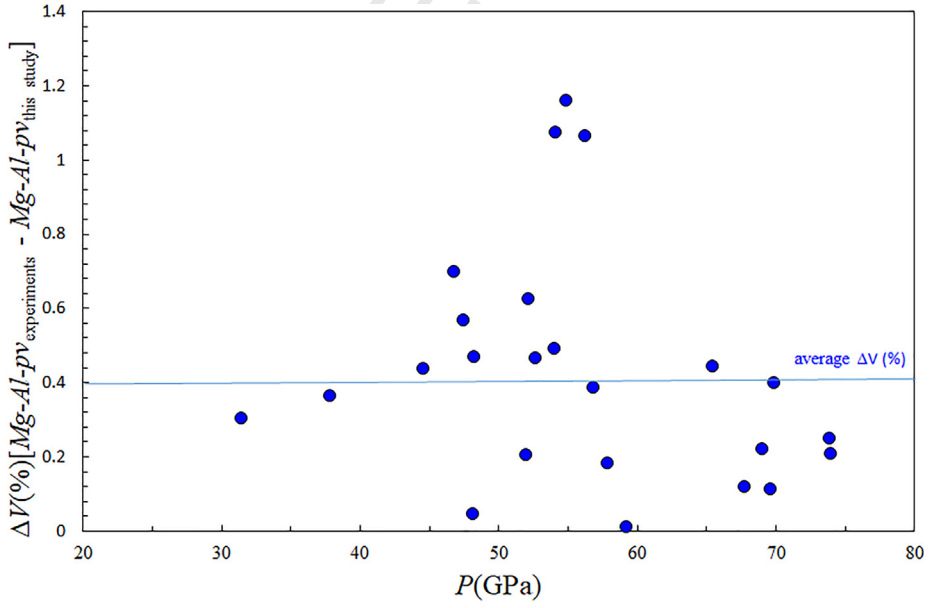


Fig. 7. Cell volume disagreement (%), between measurements and our calculations, in the case of Al bearing perovskite, as a function of $P$. Experimental values from Walter et al (2004).

Please cite this article in press as: Merli M., et al. Aluminium distribution in an Earth's *non–primitive* lower mantle. *Geochim. Cosmochim. Acta* (2020), https://doi.org/10.1016/j.gca.2020.02.023

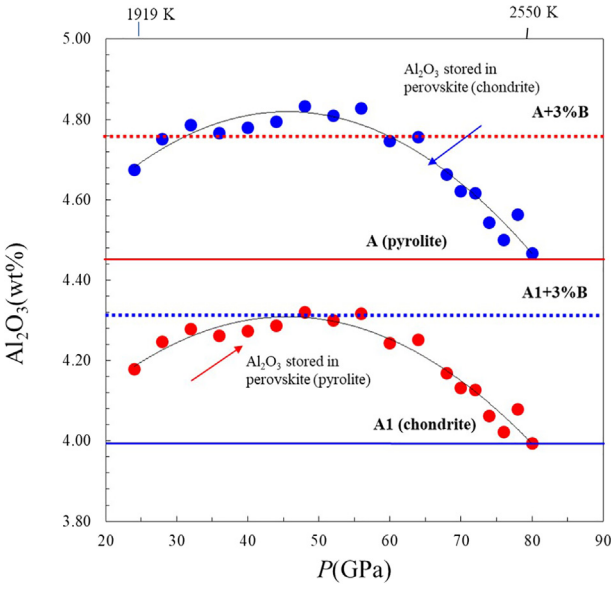


Fig. 8. The predicted *total* $Al_2O_3$ (wt%) stored in *Mg-Al-pv*, calculated by the open system model, assuming perovskite amounts of 76% (red dots) and 85% (blue dots) of the lower mantle mass, in pyrolite and chondrite reference models (Table 1), respectively. Bulk $Al_2O_3$ contents of pyrolite (A) and chondrite (A1) primitive lower mantle models are shown by red and blue solid lines, respectively. Bulk $Al_2O_3$ contents of pyrolite type and chondrite type *non-primitive* lower mantle models calculated by adding a 3 wt % of MORB component (B) are represented by red and blue dotted lines, respectively. MORB composition from Hirose et al. (1999). *P-T* region of 24–80 GPa/1919–2550 K is referred to the chosen geotherm.

The relative proportion of this phase in a lower mantle mixed with 3% of MORB-like component does not significantly vary with respect to the reference models (Table 1). This is consistent with the fact that the total *chemical probability of formation, p*(J,chem), of the Mg-rich perovskite type phases (*i.e. Mg-pv* + *Mg-Fe-pv* + *Mg-Al-pv*) does not significantly change between the primitive (A and A1) and *non-primitive* (A + 3%B and A1 + 3%B) lower mantle models (Table 2).

The predicted *total* $Al_2O_3$ that *Mg-Al-pv* may accommodate is shown in Fig. 8, along with the *bulk* Al content inferred for primitive and enriched lower mantle compositions. We point out two aspects:

(i) the average *total* $Al_2O_3$ that perovskite (76 and 85 wt % in pyrolite and chondrite reference models, respectively) hosts is 4.28 and 4.78 wt% of the lower mantle mass. Such figures prove that perovskite is able to accommodate *almost* the entire budget of $Al_2O_3$ estimated for *non-primitive* lower mantle compositions. Perovskite exhibits an average Al hosting capacity of ~90%, in the case of pyrolite model ($Al_2O_3$: 4.76 wt%), and >100%, in the case of chondrite model ($Al_2O_3$: 4.31wt%). See also Table 1 and Fig. 8;

(ii) the *total* $Al_2O_3$ stored by *Mg-Al-pv* as a function of *P-T* (Fig. 8) varies in a comparatively narrow range from 24 to about 60 GPa (~4.18–4.24 wt% and ~4.67–4.75 wt%, for pyrolite and chondrite models, respectively), while it decreases going down the mantle (3.99 and 4.47 wt%, for pyrolite and chondrite models, respectively), at 80 GPa. This may be related to the occurrence of the already mentioned change of trend exhibited by the average equilibrium constant (Fig. 2). The decrease of the $\lambda_{Al2O3}$-values (Fig. 5) and the "saturation" of the $Al_2O_3$ partitioning between perovskite and *cor* (Fig. 4) point to: i) a progressive reduction in the Al storage capacity of *Mg-Al-pv*; ii) a change of the *cor*/*Mg-Al-pv* trend that might reflect the onset of instability in perovskite, probably leading to the formation of other aluminium hosting phases (*i.e.* structural change to post perovskite; Murakami et al., 2004; Shim et al., 2008; Tsuchiya and Tsuchiya, 2008; Tateno et al., 2009). We believe that it is physically incongruous that at $P \sim 60$–80 GPa the *cor*/perovskite molar ratio inverts its decreasing trend, as this suggests that *Mg-Al-pv* loses competitiveness with respect to *cor* in hosting aluminium upon increasing *P*. In fact: (i) *cor* undergoes a phase transition to the rhodium-oxide-like phase in the range of ~80–100 GPa (Thomson et al., 1996; Funamori and Jeanloz, 1997; Merli and Pavese, 2018); (ii) the Al content in perovskite monotonically decreases with pressure (60–80 GPa; Fig. 5), thus implying a reduction of the strain, which is due to the occurrence of species other than Mg-Si. Such a reduction of the strain is expected to promote the stability of a perovskite-like structure.

Altogether, it can be observed that:

i) aluminium is *globally* incorporated foremost *via* an increase of the Al bearing perovskite amount, rather than by an increase of the $Al_2O_3$ content in *Mg-Al-pv* chemical composition;
ii) the perovskite phase is able to accommodate an Al excess consistent with 3 wt% MORB-component mixed with primitive lower mantle compositions, up to 100% and 90% of the $Al_2O_3$-budget, in the case of chondrite and pyrolite models, respectively.

At higher pressure than those investigated here, the transformations of corundum to a more stable structure (~80–100 GPa) as mentioned above and of perovskite to the $CaIrO_3$-like phase (often called post-perovskite) at ~120 GPa (Murakami et al., 2004) might account for the change of the trend related to the Al storage capacity of perovskite (Fig. 4). In fact, calculated phase equilibria in the $MgSiO_3$-$Al_2O_3$ system, modelled at *P-T* conditions relevant for the Earth's deepest mantle (80–140 GPa/2000–4000 K), predict the appearance of (Al bearing) post perovskite coexisting with Mg-perovskite between 90 and 105 GPa, at $T = 2000$ and 3000 K, respectively (Tsuchiya and Tsuchiya, 2008). According to the phase diagrams of these authors, the perovskite structure can accommodate up to ~0.19 moles of $Al_2O_3$ at 80 GPa and 2000 K, whereas at 3000 K the solubility of alumina increases up to ~0.4 moles. Interpolation yields ~0.3 moles of $Al_2O_3$ at 80 GPa and 2550 K. Such results can be compared with ours,

achieved by the closed system model, which relies on the same equilibrium thermodynamics approach. It is worth noting that the closed system model yields the $Al_2O_3$ composition of *Mg-Al-pv* that mostly shifts reaction (5) to the right, *i.e.* $K(P,T,\xi_{\text{closed system}})$ has a maximum. $\xi_{\text{closed system}}$ in turn, has an increasing trend trailing down the lower mantle (Figs. 1 and 6), providing an $Al_2O_3$ content of ~0.26 moles at $P = 80$ GPa, in agreement with Tsuchiya and Tsuchiya (2008).

### 5.2. Composition of *Mg-Al-pv* in the lower mantle

There is a controversy on whether the negative buoyancy associated with subducted oceanic crust can overcome the viscous forces in the dynamic regions of Core Mantle Boundary (CMB) and accumulate into large thermochemical piles (*i.e.* large low shear velocity provinces, LLSVP: Li and McNamara, 2018). Conversely, a general *consensus* is that most of the subducted crust is variably stirred into the background mantle and completely dissolved, in a time span that varies from 0.1 to 1 Ga (Kumari et al., 2016; White, 2015; Foley and Rizo, 2017; Yu et al., 2018).

Using the phase proportions of *Mg-pv*, *Mg-Al-pv* and *cor* as a function of the exchanged alumina according to reaction (5), we can reconstruct the probability to find *Mg-Al-pv* with a given composition in $Al_2O_3$ (*i.e. occurrence probability*: $p_o\%$). Note that $p_o\%$ must not be confused with the *chemical probability of formation*, *i.e.* $p(\text{J,chem})$, discussed in Section 3.1 which represents the mere probability to have the right oxide combination to form a given phase.

The probability of the occurrence of perovskite with low $Al_2O_3$ content *per* formula unit (0.01–0.15 mole fraction) is ~28% at 24 GPa/1919 K, and increases up to ~43% at 80 GPa/2550 K. In general, low alumina compositions (0.01–0.15 mole fractions) are dominant at any *P-T* explored (Fig. 9). On the contrary, the occurrence of *Mg-Al-pv* with high alumina contents in the range 0.19–0.30 mole fraction drops from ~9.8% to ~2%, passing from 24 GPa/1919 K to 80 GPa/2550 K, respectively. Compositions of natural Al bearing perovskite, occurring as diamond inclusions and "*claimed*" to be ascribable to the lower mantle (Kaminsky, 2012; Harte and Richardson, 2012; Harte et al., 1999), lie in the $Al_2O_3$ range associated with the largest occurrence probability (*i.e.* $p_o\%$). Leaving any opinion about their representativeness of the lower mantle mineralogy aside, there is a consistency between observations and our predictions (Fig. 9).

To conclude, *Mg-Al-pv* competes with *Mg-pv* to the phase composition of the lower mantle (Fig. 3) and the probability to find *Mg-Al-pv* in the lower mantle is almost of the same order of magnitude as *Mg-pv* (Fig. 9). In addition, the distribution of Al in *Mg-Al-pv* shows that, among the possible Al bearing perovskite phases, the $(Mg_{0.89}Al_{0.11})(Si_{0.89}Al_{0.11})O_3$ composition is the more likely, providing some 8% of the bulk perovskite at 80 GPa (Fig. 9). The occurrence of the Al richest composition, *i.e.* $(Mg_{0.71}Al_{0.29})(Si_{0.71}Al_{0.29})O_3$, is always a very rare event, *i.e.* $p_o\% < 1.7\%$.

## 6. CONCLUSIONS

We modelled the capacity of perovskite to uptake aluminium in a *non-primitive* Earth's lower mantle, because of an enrichment by 3 wt% of recycled crustal material (MORB component).

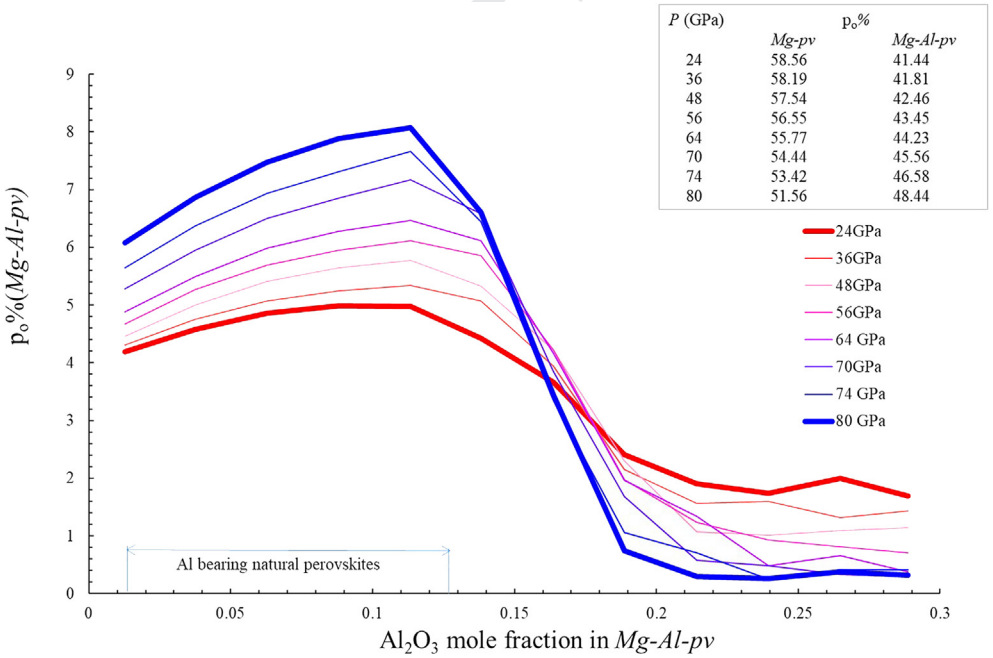


Fig. 9. Probability ($p_o\%$) of *Mg-Al-pv* occurrence with a given $Al_2O_3$ mole content *per* formula unit, according to the open system model. Each curve is associated to key *P-T* values (*P* in legend), along the chosen geotherm. The $Al_2O_3$ contents of natural Al bearing perovskite (↔) *claimed* from the lower mantle, are provided by Kaminsky and Lin (2017). In the inset table, the absolute probability to find Al bearing perovskite (*Mg-Al-pv*) against Mg-perovskite (*Mg-pv*) is reported for the explored *P-T* region of the lower mantle.

Please cite this article in press as: Merli M., et al. Aluminium distribution in an Earth's *non–primitive* lower mantle. *Geochim. Cosmochim. Acta* (2020), https://doi.org/10.1016/j.gca.2020.02.023

The investigated region stretches from 24 to 80 GPa and is geochemically described in the framework of pyrolite and chondrite reference models. The open system model used herein to predict perovskite Al incorporation capacity is independent of the geochemical framework.

Aluminium is *globally* incorporated foremost *via* an increase of the Al bearing perovskite amount [*Mg-Al-pv* (24 GPa)/*Mg-Al-pv*(80 GPa)≈1.17], rather than by an increase of the $Al_2O_3$ content in its chemical composition. At 32 GPa perovskite hosts $Al_2O_3$ at its maximum capacity ($\lambda_{Al2O3} = 0.134$ $Al_2O_3$ mole fraction) and conserves such a figure up to ~ 50 GPa; at higher pressure, a continuous decrease of $Al_2O_3$ content in *Mg-Al-pv* composition takes place up to 80 GPa ($\lambda_{Al2O3} = 0.107$ $Al_2O_3$ mole fraction).

Approaching 80 GPa, perovskite reaches some sort of "saturation" of its capacity to host aluminium, which can be considered as a prelude to instability, most likely leading to the formation of other phases (*i.e.* structural change to post perovskite) that accommodate Al. This is in keeping with the resulting phase equilibria in the $MgSiO_3$-$Al_2O_3$ system, earlier modelled at *P-T* conditions relevant for the Earth's deepest mantle (80–140 GPa/2000–4000 K).

The probability to observe a perovskite composition having an $Al_2O_3$ mole fraction up to 0.15 is about 28% at 24 GPa, increasing to 43% at 80 GPa; on the contrary, compositions in the range 0.19–0.30 $Al_2O_3$ mole fraction drop their occurrence probability from 9.8 to 2.0%. In light of this, the Al content of perovskite cannot be directly related to *P-T* conditions of formation, except that "large" $Al_2O_3$ contents suggest unlikely deep provenance, within the range explored.

The *total* $Al_2O_3$ that perovskite (amounting to 76 and 85 wt%, in pyrolite and chondrite reference models, respectively) may host is on average 4.3–4.8 wt% of the lower mantle mass. In particular, perovskite alone can account for an $Al_2O_3$ storage capacity that accommodates 100% $Al_2O_3$ predicted by a *non-primitive* chondrite model, and 90% $Al_2O_3$, forecast by a *non-primitive* pyrolite model. Calcium-ferrite type phases are possible competitors of perovskite in hosting aluminium (up to 1/5 of available Al), though their low *chemical probability of formation* likely reduces such potential. In the case of a *non-primitive* pyrolite lower mantle, Al bearing phases other than perovskite should exist, and the CF type phase is a candidate that might compensate for the 10% gap in perovskite Al incorporation capacity.

## UNCITED REFERENCES

Jie et al. (2004), Shim et al. (2018).

## ACKNOWLEDGEMENTS

This work was partly supported by PRIN-2015 20158A9CBM Grant (C.B) and PRIN 2017 - 2017L83S77 (A.P). The paper benefited from the English language editing provided by Steve Deforie and Barbara Galassi (Brighton, U.K). The Authors are indebted to the associated Editor and two anonymous Referees for their comments and suggestions, which remarkably improved the quality of the originally submitted manuscript.

## APPENDIX A

### A.1. Open and closed systems

An open system is permeable to both energy (heat and work) and matter, which are exchanged between the system and a reservoir (De Groot and Mazur, 1984; Mikhailov and Ertl, 2017). A closed system is able to exchange only energy with a reservoir. Let us assume to have a generic system in which the following reaction occurs (we restrict our discussion to one reaction only, for the sake of simplicity)

$$\sum_j \nu_j A_j = \sum_k \nu_k A_k \Rightarrow \sum_l \nu_l A_l = 0 \tag{A.a}$$

where $\{A_j\}$ and $\{A_k\}$ are "reactants and products" or "phases", which we shall term "reactants" simply. The evolution as a function of time of the $l^{th}$ reactant is given by

$$\frac{dn_l}{dt} = \nu_l \frac{d\varepsilon}{dt} + \frac{d\Delta n_l}{dt} \tag{A.b}$$

where $n_l$ means number of moles of the $l^{th}$ reactant; $\varepsilon$ is the reaction rate; the first term of the right-hand side member represents the change in $n_l$ due to the reaction (A.a); the second term accounts for a matter exchange with a reservoir.

We split the entropy of such a system into two terms (Prigogine 1968):

$$\frac{dS_{ext}}{dt} = \frac{\delta Q}{T} - \sum_l \frac{\mu_l}{T}\frac{d\Delta n_l}{dt} \tag{A.c}$$

$$\frac{dS_{int}}{dt} = -\sum_l \frac{\nu_l \mu_l}{T}\frac{d\varepsilon}{dt} \tag{A.d}$$

where $S_{ext}$ is the contribution by an exchange of heat and matter with an external reservoir; $S_{int}$ represents the entropy produced by the reaction itself. Combining Eqs. (A.b), (A.c) and (A.d), it follows that

$$\frac{dS}{dt} = \frac{\delta Q}{T} - \sum_l \frac{\nu_l \mu_l}{T}\left(\frac{d\varepsilon}{dt} + \frac{1}{\nu_l}\frac{d\Delta n_l}{dt}\right) \tag{A.e}$$

where $S$ is the total entropy. We focus our attention on *stationary* processes, which are not necessarily at equilibrium. They exhibit observables that do not change over time (Pokrovskii 2013), and therefore

$$\frac{dn_l}{dt} = 0 \tag{A.f.1}$$

$$\frac{dS}{dt} = 0 \tag{A.f.2}$$

Taking into account (A.b), (A.e) and (A.f.1), the fulfilment of the constraint (A.f.2) requires that $\delta Q = 0$. Therefore, it can be concluded that a stationary system is characterized by a possible exchange of matter with a reservoir, but not an exchange of heat.

### A.2. Open system representation

The correct treatment of a system like the one introduced above requires, in principle, to be able to formulate

explicitly both (A.c) and (A.d). Our aim is simpler, as we would like to exploit the capacity of an open system to freely exchange matter with a reservoir, in combination with a formalism as close as possible to the consolidated equilibrium thermodynamics' one. Such a model provides a flexible tool to approach problems in which one investigates the intrinsic exchanging of a *non-primitive* lower mantle capacity of a given substance, without any sort of constraint or restraint.

An internal observer (*i.e.* an observer who measures the system's observables only, unaware of the matter flow) perceives a stationary open system as one that is under equilibrium conditions ($P,T$ and $\{n_j\}$ do not change over time and $\delta Q = 0$). Therefore, all the state functions are invariant *versus* $t$ and the system conserves its composition, with possible forward/backward reactions and without any in/out flow of energy/matter. Let us represent the chemical potential of the $l^{\text{th}}$ reactant by the usual expression below,

$$\mu_l = \mu_{0l} + RTln(x_l) + RTln(\gamma_{l,int}) \tag{A.g}$$

where $\mu_{0l}$ is the component that depends on $P$-$T$ only, and coincides with the Gibbs energy of the $l^{\text{th}}$ reactant alone; $\gamma_{l,int}$ is the activity coefficient of the $l^{\text{th}}$ reactant according to the internal observer and incorporates any sort of deviation from ideal mixing.

Let us assume that $\{n_l\}$ can fluctuate, $\delta n_i$, in such a way that (A.f.1) is satisfied *on average* yet preserving the global system's composition. Therefore, the internal observer perceives that the conservation of composition is achieved through a transformation of the reactants into each other, according to the classical relationship below

$$\frac{\delta n_l}{\nu_l} = \delta\widehat{\varepsilon} \tag{A.h}$$

for any $l^{th}$ reactant; $\delta\widehat{\varepsilon}$ is the infinitesimal change of the reaction ratio, seen by the internal observer. Using the equation above, we have that

$$dG = \left[\sum_l \nu_l\mu_{0l} + RTln\left(\prod_l x_l^{\nu_l}\right) + RTln\left(\prod_l \gamma_{l,int}^{\nu_l}\right)\right]\delta\widehat{\varepsilon} \tag{A.i}$$

The internal observer states that $dG = 0$, given that the system is at equilibrium, and from (A.i) the usual chemical equilibrium equation follows

$$exp\left(-\frac{\sum_l \nu_l\mu_{0l}}{RT}\right) = \frac{\prod_k x_k^{\nu_k}}{\prod_j x_j^{\nu_j}} \times \frac{\prod_k \gamma_{k,int}^{\nu_k}}{\prod_j \gamma_{j,int}^{\nu_j}} = K(P,T)_{int} \tag{A.k}$$

An external observer (*i.e.* an observer that is aware of the matter flow) confirms that $dG = 0$ as the system lies in a stationary state, and using (A.b) expresses $dG$ in terms of

$$dG = \left[\sum_l \nu_l\mu_{0l} + RTln\left(\prod_l x_l^{\nu_l}\right) + RTln\left(\prod_l \gamma_{l,ext}^{\nu_l}\right)\right]\delta\varepsilon + \left[\sum_l \delta\Delta n_l\mu_{0l} + RTln\left(\prod_l x_l^{\delta\Delta n_l}\right) + RTln\left(\prod_l \gamma_{l,ext}^{\delta\Delta n_l}\right)\right] \tag{A.l}$$

where $\delta\Delta n_l$ is the fluctuation due to the amount of the $l^{\text{th}}$ reactant supplied by the reservoir *via* a matter flow; $\gamma_{l,ext}$ is the activity coefficient estimated by the external observer. Given that the global system's composition does not change in a stationary state, then the following relationship must hold for $\delta\Delta n_l$, too,

$$\frac{\delta\Delta n_l}{\nu_l} = \delta\zeta$$

which implies

$$dG = \left[\sum_l \nu_l\mu_{0l} + RTln\left(\prod_l x_l^{\nu_l}\right) + RTln\left(\prod_l \gamma_{l,ext}^{\nu_l}\right)\right](\delta\varepsilon + \delta\zeta) \tag{A.m}$$

Eq. (A.m), in combination with $dG = 0$, leads to an expression similar to (A.k), save the term depending on the activity coefficients, *i.e.* $\prod_l \gamma_{l,ext}^{\nu_l}$, so that

$$exp\left(-\frac{\sum_l \nu_l\mu_{0l}}{RT}\right) = \frac{\prod_k x_k^{\nu_k}}{\prod_j x_j^{\nu_j}} \times \frac{\prod_k \gamma_{k,ext}^{\nu_k}}{\prod_j \gamma_{j,ext}^{\nu_j}} = K(P,T)_{ext} \tag{A.n}$$

Therefore, the $\gamma$ activity coefficients "collect" the deviations from equilibrium that the internal and external observers detect. For (A.n) and (A.k) to coincide with one another, $\prod_l \gamma_{l,ext}^{\nu_l} = \prod_l \gamma_{l,int}^{\nu_l}$ must hold.

An open system may change its composition evolving towards a stationary state, according to the expression below, for the $l^{\text{th}}$ reactant:

$$\int_0^\infty \frac{d\Delta n_l}{dt} dt = \Delta n_l(\infty) - \Delta n_l(0)$$

where it can be assumed that at $t \to \infty$ the open system has achieved a stationary state.

### A.3. Reactant proportions and probability

What does it physically mean to neglect the activity coefficients in Eqs. (A.n) and (A.k)? Let us assume that a system has a known average Gibbs energy value, *i.e.* $\langle G\rangle$ at $P$-$T$, and that it may occupy given "states", each one with a probability $\{p_l\}$. Following a consolidated approach of statistical mechanics and information theory (Jaynes, 1957a, 1957b), we state that the likeliest and least prejudicial $\{p_l\}$-set constrained to yield $\langle G\rangle$ must correspond to an extreme of the expression beneath

$$\Phi = -R\sum_l p_l \ln(p_l) + \psi\left[\sum_l p_l G_l - < G >\right] \tag{A.o}$$

where $G_l$ is the Gibbs energy of the $l^{\text{th}}$ state; $R$ is the gas constant and $\psi$ is a lagrangian multiplier. If one requires that $\delta\Phi = 0$, then

$$p_l \propto \exp\left(-\frac{G_l}{RT}\right) \tag{A.p}$$

Taking $\psi = 1/T$. Let us shape our system in terms of a multi-phase system, in which the "states" are represented by the "reactants" that can occur. Let the system undergo a reaction like (A.a) and be composed of the related reactants. We analyse Eq. (A.a) in statistical terms. The occurrence of the left-hand or right-hand side member, can be modelled using the notion of "joint probability", thus obtaining

$$p_{left-hand\ \ side\ \ member} \propto \prod_j p_j^{\nu_j}$$

and

$$p_{right-hand\ \ side\ \ member} \propto \prod_k p_k^{\nu_k}$$

We take the ratio $p_{right\text{-}hand\ side\ member}/p_{left\text{-}hand\ side\ member}$, and observe that it can be either written as

$$\prod_l p_l^{\nu_l}$$

or formulated as

$$\prod_l \left[exp\left(-\frac{G_l}{RT}\right)\right]^{\nu_l} = exp\left(-\frac{\sum_l \nu_l G_l}{RT}\right)$$

by means of (A.p). Hence, the equations above lead to

$$\prod_l p_l^{\nu_l} = exp\left(-\frac{\sum_l \nu_l G_l}{RT}\right) \qquad \text{(A.q)}$$

Eq. (A.q) is readily likened to (A.n) and (A.k), neglecting the activity coefficients and setting for each phase $G_l \equiv \mu_{0l}$. Altogether, a chemical equilibrium equation is thus formulated in a very simple and general fashion, which holds for stationary systems, too. Therefore, neglecting the activity coefficient terms in (A.n) and (A.k) leads to revising the notion of "$l^{\text{th}}$ reactant proportion", $x_l$, in terms of "$l^{\text{th}}$ reactant occurrence probability", $p_l$, *i.e.* $x_l \equiv p_l$, once a given reaction is being considered.

## APPENDIX B

### B.1. Approximation to unity of the activity coefficients term of Eq. (7.a)

The activity coefficient term of Eq. (7.a) can be simplified as

$$\gamma = \frac{\gamma_1}{\gamma_2^{1-\lambda} \times \gamma_3^{\lambda}} \qquad \text{(B.a)}$$

where we replaced *Mg-Al-pv*, *Mg-pv* and *cor* with 1, 2 and 3, respectively. Let us introduce the geometric average of the $\gamma_{1,2,3}$s, *i.e.*

$$\gamma_{ave} = (\gamma_1 \times \gamma_2 \times \gamma_3)^{1/3}$$

and

$$\gamma_1 = \gamma_{ave} + \delta_1 \qquad \text{(B.b.1)}$$

$$\gamma_2 = \gamma_{ave} + \delta_2 \qquad \text{(B.b.2)}$$

$$\gamma_3 = \gamma_{ave} + \delta_3 \qquad \text{(B.b.3)}$$

Replacing γs in (B.a) with (B.b.1–3), then it is obtained

$$\begin{aligned}\gamma &= \frac{\left(1+\frac{\delta_1}{\gamma_{ave}}\right)}{\left(1+\frac{\delta_2}{\gamma_{ave}}\right)^{1-\lambda} \times \left(1+\frac{\delta_3}{\gamma_{ave}}\right)^{\lambda}} \\ &\approx \frac{\left(1+\frac{\delta_1}{\gamma_{ave}}\right)}{\left(1-(1-\lambda)\frac{\delta_2}{\gamma_{ave}}\right) \times \left(1-\lambda\frac{\delta_3}{\gamma_{ave}}\right)} \approx \\ &\approx \left(1+\frac{\delta_1}{\gamma_{ave}}\right) \times \left(1+(1-\lambda)\frac{\delta_2}{\gamma_{ave}}\right) \times \left(1+\lambda\frac{\delta_3}{\gamma_{ave}}\right) \\ &\approx 1 + \frac{\delta_1 + (1-\lambda)\delta_2 + \lambda\delta_3}{\gamma_{ave}} + o\left(\left(\frac{\delta}{\gamma_{ave}}\right)^2\right) \approx 1 \end{aligned} \qquad \text{(B.c)}$$

The approximation above requires $\delta/\gamma_{ave} < 1$, which holds in most cases. In fact, earlier excess enthalpy determinations on some H*P* minerals (for instance, Fe-periclase: Sreçec et al., 1987; garnets: Geiger et al., 1987; olivine: Kojitani and Akaogi, 1994; Al-perovskite: Akber-Knutson and Bukowinski, 2004; Panero et al., 2006) exhibit absolute $\Delta H$ maximum values that yield average activity coefficients [estimated by $\exp(\Delta H_{max}/RT)$, $T = 2000$ K] lying between 1.07 and 1.34, with a geometric average of 1.2 and $\langle\delta/\gamma_{ave}\rangle \sim 0.08$. Note that $\delta_1 + \delta_2(1-\lambda) + \delta_3\lambda$ is generally expected to be small as the δs compensate each other, due to $\delta_1$, $\delta_2$, and $\delta_3$ not being of the same sign. Therefore, given that we can legitimately neglect the activity coefficient in the case of Eq. (7.a), $x_l$s and $p_l$s coincide with each other, according to Appendix A.3.

## APPENDIX C. SUPPLEMENTARY MATERIAL

Supplementary data to this article can be found online at https://doi.org/10.1016/j.gca.2020.02.023.

## REFERENCES

Akber-Knutson S. and Bukowinski M. S. T. (2004) The energetics of aluminium solubility into $MgSiO_3$ perovskite at lower mantle conditions. *Earth Planet. Sci. Lett.* **220**, 317–330.

Akber-Knutson S., Steinle-Neumann G. and Asimow P. D. (2005) Effect of Al on the sharpness of the $MgSiO_3$ perovskite to post-perovskite phase transition. *Geophys. Res. Lett.* **32**, L14303.

Anderson D. L. (1989) Composition of the Earth. *Science* **243**, 367–370.

Badro J., Cote A. S. and Brodholt J. P. (2014) A seismologically consistent compositional model of Earth's core. *Proc. Nat. Acad. Sci. USA* **111**, 7542–7545.

Baker J. A., Schiller M. and Bizzarro M. (2012) 26Al-26Mg deficit dating ultramafic meteorites and silicate planetesimal differentiation in the early Solar System?. *Geochim. et Cosmochim. Acta* **77** 415–431.

Ballmer M. D., Houser C., Hernlund J. W., Wentzcovitch R. M. and Hirose K. (2017) Persistence of strong silica-enriched domains in the Earth's lower mantle. *Nat. Geosci.*. https://doi.org/10.1038/NGEO2898.

Billen M. I. (2010) Slab dynamics in the transition zone. *Phys. Earth Planet. Inter.* **183**, 296–308.

Brown J. M. and Shankland T. J. (1981) Thermodynamic parameters in the Earth as determined from seismic profiles. *Geoph. J. Royal Astronom. Soc.* **66**, 579–596.

Christensen U. R. and Yuen D. A. (1984) The interaction of a subducting lithospheric slab with a chemical or phase boundary. *J. Geophys. Res.* **89**, 4389–4402.

Christensen U. R. and Hofmann A. W. (1994) Segregation of subducted oceanic crust in the convecting mantle. *J. Geophys. Res.* **99**.

Bina C. R. and Helffrich G. (2014) Geophysical Constraints on Mantle Composition. In *Treatise on Geochemistry*, Vol. 3 (eds. H. D. Holland and K. K. Turekian). Elsevier, Oxford, pp. 41–65.

Bizzarro M., Baker J., Haack H. and Lundgaard K. (2005) Rapid timescales for accretion and melting of differentiated planetesimals inferred from $^{26}Al$–$^{26}Mg$ chronometry. *Astrophys. J.* **632**, L42–L44.

Burton B. P. and van de Walle A. (2003) First principles based calculations of the CaCO3–MgCO3 subsolidus phase diagrams. *Phys. Chem. Miner.* **30**, 88–97.

Catti M., Valerio G., Dovesi R. and Causà M. (1994) Quantum-mechanical calculation of the solid-state equilibrium MgO+α-$Al_2O_3$⇄$MgAl_2O_4$ (spinel) versus pressure. *Phys. Rev. B* **49**, 14179.

Causà M., Dovesi R., Pisani C. and Roetti C. (1986) Electronic structure and stability of different crystal phases of magnesium oxide. *Phys. Rev. B* **33**, 1308–1316.

Chust T. C., Steinle-Neumann G., Dolejš D., Schuberth B. S. A. and Bunge H. P. (2017) MMA-EoS: A computational framework for mineralogical thermodynamics. *J. Geophys. Res.: Solid Earth* **122**, 9881–9920. https://doi.org/10.1002/2017JB014501.

Corà F. (2005) The performance of hybrid density functionals in solid state chemistry: the case of BaTiO3. *Mol. Phys.* **103**, 2483–2496.

De Groot S. R. and Mazur P. (1984) Non-equilibrium thermodynamics. Dover Publications.

Dovesi R., Saunders V. R., Roetti C., Orlando R., Zicovich-Wilson C. M., Pascale F., Civalleri B., Doll K., Harrison N. M., Bush I. J., D'Arco P. and Llunell M. (2009) CRYSTAL09 user's manual. University of Torino, IT, Torino.

Faure G. (1986) Principles of Isotopic Geology. Wiley, New York.

Foley B. J. and Rizo H. (2017) Long-term preservation of early formed mantle heterogeneity by mobile lid convection: Importance of grainsize evolution. *Earth Planet. Sci. Lett.* **475**, 94–105.

Fukuyama K., Ohtani E., Shibazaki Y., Kagi H. and Suzuki A. (2017) Stability field of phase Egg, $AlSiO_3OH$ at high pressure and high temperature: possible water reservoir in mantle transition zone. *J. Mineral. Petrol. Sci.* **112**, 31–35.

Funamori N. and Jeanloz R. (1997) High-Pressure Transformation of $Al_2O_3$. *Science* **278**, 1109–1111. https://doi.org/10.1126/science.278.5340.1109.

Funamori N., Jeanloz R., Miyajima N. and Fujino K. (2000) Mineral assemblages of basalt in the lower mantle. *J. Geophys. Res.* **105**, 26037–26043. https://doi.org/10.1029/2000JB900252.

Gale A., Dalton C. A., Langmuir C. H., Su Y. and Schilling J.-G. (2013) The mean composition of ocean ridge basalts. *Geochem. Geophys. Geosyst.* **14**, 489–518. https://doi.org/10.1029/2012GC004334.

Gale J. D. (1997) GULP-a computer program for the symmetry adapted simulation of solids. *JCS Faraday Trans* **93**, 629–637.

Gale J. D. (2005) GULP: Capabilities and prospects. *Z. Krist.* **220**, 552–554.

Gasparik T., Tripathi A. and Parise J. B. (2000) Structure of a new Al-rich phase, [K, Na]0.9[Mg, Fe]2[Mg, Fe, Al, Si]6O12, synthesized at 24 GPa. *Am. Mineral.* **85**, 613–618.

Geiger C. A., Newton R. C. and Kleppa O. J. (1987) Enthalpy of mixing of synthetic almandine-grossular and almandine-pyrope garnets from high-temperature solution calorimetry. *Geochim. Cosmochim. Acta* **51**, 1755–1763.

Ghosh S. and Schmidt M. W. (2014) Melting of phase D in the lower mantle and implications for recycling and storage of H2O in the deep mantle. *Geochim. Cosmochim. Acta* **145**, 72–88.

Guignot N. and Andrault D. (2004) Equations of state of Na–K–Al host phases and implications for MORB density in the lower mantle. *Phys Earth Planet. Int.* **143–144**, 107–128.

Harte B. and Richardson S. (2012) Mineral inclusions in diamonds track the evolution of a Mesozoic subducted slab beneath West Gondwanaland. *Gond. Res.* **21**, 236–245.

Harte B., Harris J. W., Hutchison M. T., Watt G. R. and Wilding M. C. (1999) Lower mantle mineral associations in diamonds from Sao Luiz, Brazil No 6. In *Mantle Petrology: Field Observations and High Pressure Experimentation; a tribute to Francis R. (Joe) Boyd* (eds. Y. Fei, C. M. Bertka and B. O. Mysen). The Geochemical Society Special Publication, pp. 125–153.

Hirose K., Fei Y., Ma Y. and Mao H.-K. (1999) The fate of subducted basaltic crust in the Earth's lower mantle. *Nature* **397**, 53–56.

Hirose K., Takafuji N., Nagayoshi S. and Ohishi Y. (2005) Phase transition and density of subducted MORB crust in the lower mantle. *Earth Planet. Sci. Lett.* **237**, 239–251.

Honda S. (2017) Geodynamic modeling of the subduction zone around the Japanese Islands. *Monogr. Environ. Earth Planets* **5** (2), 35–62.

Imada S., Hirose K., Komabayashi T., Suzuki T. and Ohishi Y. (2012) Compression of $Na_{0.4}Mg_{0.6}Al_{1.6}Si_{0.4}O_4$ NAL and Ca-ferrite-type phases. *Phys. Chem. Min.* **39**, 525–530.

Imada S., Hirose K. and Ohishi Y. (2011) Stability of NAL and Ca-ferrite-type phases on the join $NaAlSiO_4$-$MgAl_2O_4$. *Phys. Chem. Min.* **38**, 557–560.

Ismailova L., Bykova E., Bykov M., Cerantola V., McCammon C., Boffa Ballaran T., Bobrov A., Sinmyo R., Dubrovinskaia N., Glazyrin K., Liermann H. P., Kupenko I., Hanfland M., Prescher C., Prakapenka V., Svitlyk V. and Dubrovinsky L. (2016) Sgtability of Fe, Al-bearing bridgmanite in the lower mantle and synthesis of pure Fe-bridgmanite. *Sci. Adv.* **2**, e1600427.

Irifune T. and Ringwood A. E. (1993) Phase transformations insubducted oceanic crust and buoyancy relationships at depth of 600–800 km in the mantle. *Earth Planet. Sci.* **117**, 101–110.

Irifune T., Shinmei T., McCammon C. A., Miyajima N., Rubie D. C. and Frost D. J. (2010) Iron partitioning and density changes of pyrolite in Earth's lower mantle. *Science* **327**, 193–195.

Irifune T., Fujino K. and Ohtani E. (1991) A new high-pressure form of $MgAl_2O_4$. *Nature* **349**, 409–411.

Irifune T., Koizumi T. and Ando J. I. (1996) An experimental study of the garnet–perovskite transformation in the system $MgSiO_3$–$Mg_3Al_2Si_3O_{12}$. *Phys. Earth Planet. In.* **96**, 147–157. https://doi.org/10.1016/0031-9201(96)03147-0.

Jaynes E. T. (1957a) Information Theory and Statistical Mechanics (PDF). *Phys. Rev. Ser. II* **106**, 620–630.

Jaynes E. T. (1957b) Information Theory and Statistical Mechanics (PDF). *Phys. Rev. Ser. II* **108**, 171–190.

Javoy M., Kaminski E., Guyot F., Andrault D., Sanloup C., Moreira M., Labrosse S., Jambon A., Agrinier P., Davaille A. and Jaupart C. (2010) The chemical composition of the Earth: Enstatite chondrite models. *Earth and Planet. Sci. Lett* **293**, 259–268. https://doi.org/10.1016/j.epsl.2010.02.033.

Jeanloz R. and Knittle E. (1989) Density and composition of the lower mantle. *Phil. Trans. Royal Soc Lon.* **A328**(1599), 377–389. https://doi.org/10.1098/rsta.1989.0042.

van Jones R. E., Keken P. E., Hauri E., Tucker J. M., Vervoort J. and Ballentine C. J. (2019) Origins of the terrestrial Hf-Nd mantle array: Evidence from a combined geodynamical-geochemical approach. *Earth and Planet. Sci. Lett* **518**, 26–39.

Kaminski E. and Javoy M. (2013) A two-stage scenario for the formation of the Earth's mantle and core. *Earth Planet. Sci. Lett.* **365**, 97–107.

Kaminsky F. (2012) Mineralogy of the lower mantle: a review of super-deep mineral inclusions in diamond. *Earth Sci. Rev.* **110**, 127–147.

Kaminsky F. and Lin J.-F. (2017) Iron partitioning in lower mantle minerals: toward a chemically heterogeneous lower mantle. *Am Miner.* **102**, 824–832.

Kato C., Hirose K., Komabayashi T., Ozawa H. and Ohishi Y. (2013) NAL phase in K-rich portions of the lower mantle. *J. Geophys. Res.* **40**, 5085–5088.

King S. D., Frost D. J. and Rubie D. C. (2015) Why cold slabs stagnate in the transition zone. *Geology* **43**, 231–234.

Kojitani H. and Akaogi M. (1994) Calorimetric study of olivine solid solutions in the system $Mg_2SiO_4$-$Fe_2SiO_4$. *Phys. Chem. Miner.* **20**, 536–540.

Korenaga J. (2009) A method to estimate the composition of the bulk silicate Earth in the presence of a hidden geochemical reservoir. *Geochim. Cosmochim. Acta* **73**, 6952–6964.

Kröger F. A. (1972) The Chemistry of Imperfect Crystals. North-Holland, Amsterdam.

Kumari S., Paul D. and Stracke A. (2016) Open system models of isotopic evolution in Earth's silicate reservoirs: Implications for crustal growth and mantle heterogeneity. *Geochim. Cosmochim. Acta* **195**, 142–157.

Kurnosov A., Marquardt H., Frost D. J., Boffa Ballaran T. and Ziberna L. (2017) Evidence for a $Fe^{3+}$-rich pyrolytic lower mantle from (Al, Fe)-bearing bridgmanite elastic data. *Nature* **543**, 543–546.

Lee T., Papanastassiou D. A. and Wasserburg G. J. (1977) Al-26 in the early Solar-System – fossil or fuel. *Astrophys. J.* **211**, L107–L110.

Jie Li J., Viktor V., Struzhkin V. V., Mao H-, Shu J., Hemley R. J., Fei Y., Mysen B., Dera P., Prakapenka V. and Shen G. (2004) Electronic spin state of iron in lower mantle perovskite. *Proc. Nat. Acad. Sci. USA* **101**, 14027–14030.

Li L., Weidner D. J., Brodholt J., Alfè D. and Price G. D. (2008) Ab initio molecular dynamics study of elasticity of akimotoite $MgSiO_3$ at mantle conditions. *Phys. Earth Planet. Inter.* **173**, 115–120.

Li M. and McNamara A. K. (2013) The difficulty for subducted oceanic crust to accumulate at the Earth's core-mantle boundary. *J. Geophys. Res. Solid Earth* **118**, 1807–1816. https://doi.org/10.1002/jgrb.50156.

Li M. and McNamara A. K. (2018) The influence of deep mantle compositional heterogeneity on Earth's thermal evolution. *Earth Planet. Sc. Lett.* **500**, 86–96.

Litasov K. D. and Ohtani E. (2007) Effect of water on the phase relations in Earth's mantle and deep water cycle. *Spec. Paper Geolog. Soc. Am.* **421**, 115–156. https://doi.org/10.1130/2007.2421(08).

Lodders K. (2003) Solar system abundances and condensation temperatures of the elements. *Astrophys. J.* **591**, 220–1247.

Lodders K., Palme H. and Gail H.-P. (2009) Abundances of the elements in the solar system. In *Astronomy and Astrophysics*, Vol. VI/4B (ed. J. E. Trumper). , Springer-Verlag, Landolt-Bornstein, New Series Berlin, pp. 560–630.

Lyubetskaya T. and Korenaga J. (2007) Chemical composition of Earth's primitive mantle and its variance. *J. Geoph. Res.* **112**, B03211. https://doi.org/10.1029/2005JB004223.

Mahan B., Siebert J., Blanchard I., Borensztajn S., Badro J. and Moynier F. (2018) Constraining compositional proxies for Earth's accretion and core formation through high pressure and high temperature Zn and S metal-silicate partitioning. *Geochim. Cosmochim. Acta* **235**, 21–40.

Marty B. (2012) The origins and concentrations of water, carbon, nitrogen and noble gases on Earth. *Earth Planet. Sci. Lett.* **313**, 56–66.

Mattern E., Matas J., Ricard Y. and Bass J. (2005) Lower mantle composition and temperature from mineral physics and thermodynamic modelling. *Geophys. J. Int.* **160**, 973–990.

McDonough W. F. and Sun S.-S. (1995) The composition of the Earth. *Chem. Geol.* **120**, 223–253.

McDonough W. F. (2014) Compositional model for the Earth's core. In *The Mantle and Core* (ed. R. W. Carlson). Elsevier, Amsterdam, pp. 559–577.

Merli M. and Pavese A. (2018) Electron-density critical points analysis and catastrophe theory to forecast structure instability in periodic solids. *Acta Crystallogr. Sect. A: Found. Adv.* **74**, 102–111.

Merli M., Sciascia L., Pavese A. and Diella V. (2015) Modelling of thermo-chemical properties over the sub-solidus MgO–FeO binary, as a function of iron spin configuration, composition and temperature. *Phys. Chem. Min.* **42**, 347–362.

Merli M., Bonadiman C., Diella V. and Pavese A. (2016) Lower mantle hydrogen partitioning between periclase and perovskite: A quantum chemical modelling. *Geoch. Cosmochim. Acta* **173**, 304–318.

Merli M., Bonadiman C., Diella V., Sciascia L. and Pavese A. (2017) Fe-periclase reactivity at Earth's lower mantle conditions: *ab-initio* geochemical modelling. *Geochim. Cosmochim. Acta* **214**, 14–29.

Mikhailov A. S. and Ertl G. (2017) Thermodynamics of Open Systems. *Chemical Complexity. The Frontiers Collection*. Springer, Cham.

Mohn C. E. and Trønnes R. (2016) Iron spin state and site distribution in FeAlO3-bearing bridgmanite. *Earth Plan. Sci. Lett.* **440**, 178–186.

Murakami M., Hirose K., Kawamura K., Sata N. and Ohishi Y. (2004) Post-perovskite phase transition in $MgSiO_3$. *Science* **304**, 855–858.

Muir J. M. R. and Brodholt J. P. (2018) Water distribution in the lower mantle: Implications for hydrolytic weakening. *Earth Plan. Sci. Lett.* **484**, 363–369. https://doi.org/10.1016/j.epsl.2017.11.051.

Murakami M., Ohishi Y., Hirao N. and Hirose K. (2012) A perovskitic lower mantle inferred from high-pressure, high-temperature sound velocity data. *Nature* **485**, 90–95.

Navrotsky A., Schoenitz M., Kojitani H., Xu H., Zhang J., Weidner D. J. and Jeanloz R. (2003) Aluminium in magnesium silicate perovskite: Formation, structure, and energetics of magnesium-rich defect solid solutions. *J. Geophys. Res.* **108** (B7), 2330. https://doi.org/10.1029/2002JB002055.

Nestola F., Korolev N., Kopylova M., Rotiroti N., Pearson D. G., Pamato M. G., Alvaro M., Peruzzo L., Gurney J. J., Moore A. E. and Davidson J. (2018) $CaSiO_3$ perovskite in diamond indicates the recycling of oceanic crust into the lower mantle. *Nature* **555**, 237–241.

Nishio-Hamane D., Nagai T., Fujino K., Seto Y. and Takafuji N. (2005) $Fe^{3+}$ and Al solubilities in $MgSiO_3$ perovskite: implication of the $Fe^{3+}$AlO3 substitution in $MgSiO_3$ perovskite at the lower mantle condition. *Geophy. Res. Lett.* **32**, L16306.

Nolet G., Allen R. and Zhao D. (2007) Mantle plume tomography. *Chem. Geol.* **241**, 248–263.

Norris T. L., Gancarz A. J., Rokop D. J. and Thomas K. W. (1983) Half-life of $^{26}$Al. *J. Geophys. Res.* **88**(S1), B331–B333.

Ohtani E., Litasov K., Suzuki A. and Kondo T. (2001) Stability field of new hydrous phase, δ-AlOOH, with implications for water transport into the deep mantle. *Geophys. Res. Lett.* **28**, 3991–3993.

Ohtani E., Amaike Y., Kamada S., Sakamaki T. and Hirao N. (2014) Stability of hydrous phase H $MgSiO_4H_2$ under lower mantle conditions. *Geophys. Res. Lett.* **41**, 8283–8287.

Ottonello G. (1997) *Principles of Geochemistry*. Columbia University Press, New York.

Ottonello G., Civalleri B., Ganguly J., Perger W. F., Belmonte D. and Vetuschi Zuccolini M. (2010) Thermo-chemical and thermos-physical properties of the high pressure phase Anhydrous B ($Mg_{14}Si_5O_{24}$): an *ab initio* all-electron investigation. *Am. Mineral.* **95**, 563–573.

Palme H. and Oneill H. (2014) Cosmochemical estimates of mantle composition. In *Treatise on Geochemistry*, Vol. 3 (ed. R. W. Carlson). Elsevier, Oxford, pp. 1–39.

Pamato M. G., Myhill R., Boffa Ballaran T., Frost D. J., Heidelbach F. and Miyajima N. (2015) Lower-mantle water reservoir implied by the extreme stability of a hydrous aluminosilicate. *Nat. Geosci.* **8**, 75–79.

Panero W. R., Akber-Knutson S. and Stixrude L. (2006) $Al_2O_3$ incorporation in MgSiO3 perovskite and ilmenite. *Earth Planet. Sci. Lett.* **252**, 152–161.

PetDB Petrological Database (https://www.earthchem.org/petdb).

Prigogine I. (1968) *Introduction to thermodynamics of irreversible processes*, third ed. John Wiley & Sons Inc, N.Y., p. 9.

Pokrovskii V. N. (2013) A derivations of the main relations of non-equilibrium thermodynamics. *IRSN Thermodyn.* **906136**, 9. https://doi.org/10.1155/2013/906136.

Ricolleau A., Fiquet G., Addad A., Menguy N., Vanni C., Perrillat J. P., Daniel I., Cardon H. and Guignot N. (2008) Analytical transmission electron microscopy study of a natural MORB sample assemblage transformed at high pressure and high temperature. *Am. Min.* **93**, 144–153. https://doi.org/10.2138/am.2008.2532.

Ricolleau A., Fei Y., Cottrell E., Watson H. C., Deng L., Zhang L., Fiquet G., Auzende A.-L., Roskosz M., Morard G. and Prakapenka V. (2009) Density profile of perovskite under the lower mantle conditions. *Geophys. Res. Lett.* **36**, L06302.

Ricolleau A., Perrillat J. P., Fiquet G., Daniel I., Matas J., Addad A., Menguy N., Cardon H., Mezouar M. and Guignot N. (2010) Phase relations and equation of state of a natural MORB: Implications for the density profile of subducted oceanic crust in the Earth's lower mantle. *J. Geophys. Res.* **115**, B08202.

Shim S.-H., Catalli K., Hustoft J., Kubo A., Prakapenka V. B., Caldwell W. A. and Kunz M. (2018) Crystal structure and thermoelastic properties of $(Mg_{0.91}Fe_{0.09})SiO_3$ postperovskite up to 135 GPa and 2,700 K. *Proc. Nat. Acad. Sci. USA* **105**, 7382–7386.

Sreçec I., Ender A., Woermann E., Gans W., Jacobsson E., Eriksson G. and Rosen E. (1987) Activity-composition relations of the magnesiowüstite solid solution series in equilibrium with metallic iron in the temperature range 1050–1400 K. *Phys. Chem. Miner.* **14**, 492–498.

Sigloch K., McQuarrie N. and Nolet G. (2008) Two-stage subduction history under North America inferred from multiple-frequency tomography. *Nat. Geosci.* **1**, 458–462. https://doi.org/10.1038/ngeo231.

Spivak-Birndorf M. and Wadhwa P. Janne (2009) 26Al–26Mg systematics in D'Orbigny and Sahara 99555 angrites: implications for high-resolution chronology using extinct chronometers. *Geochim. Cosmochim. Acta* **73**, 5202–5211.

Stebbins J. F., Kroeker S. and Andrault D. (2001) The mechanism of solution of aluminium oxide in MgSiO3 perovskite. *Geophys. Res. Lett.* **28**, 615–618.

Stixrude L. and Lithgow-Bertelloni C. (2005) Thermodynamics of mantle minerals—I. Physical properties. *Geophys. J. Int.* **162**, 610–632.

Stixrude L. and Lithgow-Bertelloni C. (2012) Geophysics of chemical heterogeneity in the mantle. *Ann. Rev. Earth Planet. Sci. Lett.* **40**, 569–595.

Tateno S., Hiros K., Sata N. and Ohishi Y. (2009) Determination of post-perovskite phase transition boundary up to 4400K and implications for thermal structure in D"layer. *Earth Planet. Sci. Lett.* **277**, 130–136.

Thomson K. T., Wentzcovitch R. M. and Bukowinski M. S. T. (1996) Polymorphs of alumina predicted by first principles: putting pressure on the ruby pressure scale. *Science* **274**, 1880–1882.

Towler M., 2015. CRYSTAL Resources Page. Theory of Condensed Matter http://www.tcm.phy.cam.ac.uk/~mdt26/crystal.html.

Tschauner O., Ma C., Prescherb C. and Prakapenka V. B. (2018) Structure analysis and conditions of formation of akimotoite in the Tenham chondrite. *Meteor. Planet. Sci* **53**, 62–74.

Tsuchiya J. and Tsuchiya T. (2008) Post-perovskite phase equilibria in the $MgSiO_3$-$Al_2O_3$ system. *Proc. Nat. Acad. Sci. USA* **105**, 19160–19164.

Valencia-Cardona J. J., Shukla G., Wu Z., Houser C., Yuen D. A. and Wentzcovitch R. M. (2017) Influence of the iron spin crossover in ferropericlase on the lower mantle geotherm. *Geophys. Res. Lett.* **44**, 4863–4871. https://doi.org/10.1002/2017GL073294.

van der Hilst R. D., Widiyantoro S. and Engdahl E. R. (1997) Evidence for deep mantle circulation from global tomography. *Nature* **386**, 578–584.

van de Walle A. and Ceder G. (2002) The effect of lattice vibrations on substitutional alloy thermodynamics. *Rev. Mod. Phys.* **74**, 11–45.

Walter M. J., Kubo A., Yoshino T., Brodholt J. P., Koga K. T. and Ohishi Y. (2004) Phase relations and equation-of-state of aluminous Mg-silicate perovskite and implications for Earth's lower mantle. *Earth Planet. Sci. Lett.* **222**, 501–516.

Walter M. J., Thomson A. R., Wanga W., Lord O. T., Ross J., McMahon S. C., Baron M. A., Melekhova E., Kleppe A. K. and Kohn S. C. (2015) The stability of hydrous silicates in Earth's lower mantle: Experimental constraints from the systems MgO–$SiO_2$–$H_2O$ and MgO–$Al_2O_3$–$SiO_2$–$H_2O$. *Chem. Geol.* **418**, 16–29.

Wang K. and Jacobsen S. B. (2016) An estimate of the Bulk Silicate Earth potassium isotopic composition based on MC-ICPMS measurements of basalts. *Geochim. Cosmochim. Acta* **173**, 223–232.

Wang X., Tsuchiya T. and Hase A. (2015) Computational support for a pyrolitic lower mantle containing ferric iron. *Nat. Geosci.* **8**, 556–559. https://doi.org/10.1038/ngeo2458.

Wasson J. T. and Kallemeyn G. W. (1988) Compositions of chondrites. *Philos. Trans. R. Soc. London Ser. A* **325**, 535–544.

White W. M. (2015) Probing the Earth's deep interior through geochemistry. *Geochem. Perspect.* **4**(2), 95–251.

Wimpenny J., Sanborn M. E., Koefoed P., Cooke I. R., Stirling C., Amelin Y. and Qing-Zhu Yin Q.-Z. (2019) Reassessing the origin and chronology of the unique achondrite Asuka 881394: Implications for distribution of 26Al in the early Solar System. *Geochim. Cosmochim. Acta* **244**, 478–501.

Wu Y., Wu X., Lin J., McCammon C. A., Xiao Y., Chow P., Prakapenka V. B., Yoshino T., Zhai S. and Qin S. (2016) Spin transition of ferric iron in the NAL phase: Implications for the seismic heterogeneities of subducted slabs in the lower mantle. *Earth Planet. Sci. Lett.* **434**, 91–100.

Wu, S.C., Browne, E., 1997. Comments on evaluation of 26Al electron-capture and position decay data. Comments on Evaluation CEA. ISBN 2 7272 0211 3.

Wu Z. and Cohen R. E. (2006) More accurate generalized gradient approximation for solids. *Phys. Rev. B* **73**, 235116.

Yamamoto T., Yuen D. A. and Ebisuzaki T. (2003) Substitution mechanism of Al ions in $MgSiO_3$ perovskite under high pressure conditions from first-principles calculations. *Earth Planet. Sci. Lett.* **206**, 617–625.

Young E. D., Simon J. I., Galy A., Russell S. S., Tonui E. and Lovera O. (2005) Supra-canonical $^{26}Al/^{27}Al$ and the residence time of CAIs in the solar protoplanetary disk. *Science* **308**, 5719.

Yu C., Day E. A., de Hoop M. V., Campillo M., Goes S., Blythe R. A. and van der Hilst R. D. (2018) Compositional heterogeneity near the base of the mantle transition zone beneath Hawaii. *Nat. Comm.* **9**, 1266.

Zhang F. and Oganov A. R. (2006) Mechanisms of $Al^{3+}$ incorporation in $MgSiO_3$ post-perovskite at high pressures. *Earth Planet. Sci. Lett.* **248**, 69–76.

Fukao Y. and Obayashi M. (2013) Subducted slabs stagnant above, penetrating through, and trapped below the 660 km discontinuity. *J. Geophys. Res.* **118**(5920), 5938.

*Associate editor:* Michael J. Toplis